J. Fluid Mech. (2011), *vol.* 682, *pp.* 332–361. © Cambridge University Press 2011
doi:10.1017/jfm.2011.228

Structural stability theory of two-dimensional fluid flow under stochastic forcing

NIKOLAOS A. BAKAS†‡ AND PETROS J. IOANNOU

Department of Physics, National and Kapodistrian University of Athens, Office 32, Building IV, Panepistimiopolis, 15784 Athens, Greece

(Received 20 May 2010; revised 18 January 2011; accepted 15 May 2011; first published online 15 July 2011)

Large-scale mean flows often emerge in turbulent fluids. In this work, we formulate a stability theory, the stochastic structural stability theory (SSST), for the emergence of jets under external random excitation. We analytically investigate the structural stability of a two-dimensional homogeneous fluid enclosed in a channel and subjected to homogeneous random forcing. We show that two generic competing mechanisms control the instability that gives rise to the emergence of an infinitesimal jet: advection of the eddy vorticity by the mean flow that is shown to be jet forming and advection of the vorticity gradient of the jet by the eddies that is shown to hinder the formation of the mean flow. We show that stochastic forcing with small streamwise coherence and an amplitude larger than a certain threshold leads to the emergence of jets in the channel through a bifurcation of the non-linear SSST system.

Key words: general fluid mechanics, instability, turbulent flows

1. Introduction

Large-scale jets that are maintained by their eddy field are commonly observed in turbulent flows. Prominent geophysical examples are the large streamwise flows that are observed in the upper atmosphere of the gaseous planets and the Earth's polar front jet. Examples from laboratory experiments include the strong jets in the vicinity of the boundaries of channels in turbulent convection (Krishnamurti & Howard 1981), the driving by convection of banded jets in rotating tank experiments (Read *et al.* 2004) and the emergence of streamwise flows in fusion plasma devices (Fujisawa *et al.* 2008). Analysis of the velocity fields and theoretical arguments have demonstrated that these jets are maintained by the Reynolds stresses of the eddy field with which they coexist (Jeffreys 1926; Kuo 1951; Starr 1968; Ingersoll 1990; Diamond *et al.* 2005; Vasavada & Showman 2005; Read *et al.* 2007).

These large-scale flows are complex, time-dependent solutions of the Navier–Stokes equations and even though they exhibit a great degree of stationarity, they are not stationary points of the equations. Consequently, in order to treat the stability of these turbulent flows, the classical stability theory originating from the pioneering work of Rayleigh (1880) has to be extended. The reason is that it only treats stationary mean flows that are maintained by an external thermal or pressure gradient. Formulation of such an extended theory requires two main components. The first component is a

† Email address for correspondence: nikos.bakas@gmail.com
‡ Present address: National and Kapodistrian University of Athens, Build. IV office 32, Panepistimiopolis, Zografos, Athens, Greece.

https://doi.org/10.1017/jfm.2011.228 Published online by Cambridge University Press

definition of what is meant by an equilibrium in these turbulent fluids. The second component is a method to obtain the structure of the turbulence and the associated Reynolds stresses, as well as model the eddy influence on the mean flow.

A framework that provides a method for formulating and calculating the stability of mean flows in turbulence is stochastic structural stability theory (hereafter SSST) developed by Farrell & Ioannou (2003). In the context of SSST, equilibria are neither defined as fixed points of the field equations alone (as in Charney & DeVore 1979; Pierrehumbert & Malguzzi 1984; Legras & Ghil 1985; Marshall & Molteni 1993; Dijkstra & Katsman 1997; Simonnet, Ghil & Dijkstra 2005 for geophysical flows, or as in Faisst & Eckhardt 2003; Waleffe 2003; Wedin & Kerswell 2004; Duguet, Schlatter & Henningson 2009 for laboratory flows) nor as maximum entropy structures (Robert & Sommeria 1991; Bouchet & Sommeria 2002). The equilibria are instead fixed points of a set of autonomous statistical dynamical equations for the average eddy-mean flow interaction and the associated evolution of the average eddy field. The average can be defined in various ways depending on the physical situation. Most comprehensively, a time average is considered over a time-scale intermediate between the fast time scale of the eddies and the slow time scale of the evolution of the large-scale flow. In this work, we will consider channel flows and will employ averages in the streamwise direction parallel to the channel boundaries.

Regarding the generation of mean flows in turbulent fluids, there are three main approaches: the cascade theory of Rhines (Rhines 1975), modulational instability (Gill 1974; Lorenz 1974) and formation of mean flows from interaction of eddies with the large-scale mean shear. The first approach starts with the pioneering work of Rhines (Rhines 1975) on turbulence on a β plane. Rhines (1975) proposed that nonlinear eddy–eddy interactions lead to an inverse energy cascade that is 'arrested' by weakly interacting Rossby waves. Because β has a stronger effect on eddies that are elongated along the cross-stream axis, the 'arrest' is anisotropic in wavenumber space and allows the upscale energy transfer to a streamwise flow (Vallis & Maltrud 1993; Nazarenko & Quinn 2009). However, observations of quasi-geostrophic turbulence in the atmospheric midlatitude jet (Shepherd 1987) and numerical analysis of simulations (Nozawa & Yoden 1997; Huang & Robinson 1998; Huang, Galperin & Sukoriansky 2001; Berloff, Kamenkovich & Pedlosky 2009*a*, *b*) showed that the energy transfer between the eddies and the streamwise jet is spectrally nonlocal. Huang & Robinson (1998) found that even though the large-scale eddies at the Rhines scale interact with the streamwise jet on short time scales, they contribute little to the net maintenance of the mean flow. The reason is that in the long-term, this interaction is statistically incoherent and averages to nearly zero in the time mean. Huang & Robinson (1998) demonstrated that the mean flows are instead maintained from the non-local interaction between the mean flow and eddies with scales smaller than the Rhines scale.

One such non-local theory for the generation of mean flows is modulational instability in which a primary meridional Rossby wave of finite amplitude transfers its energy directly to the mean flow (Gill 1974; Lorenz 1974; Connaughton *et al.* 2010). Recently, Berloff *et al.* (2009*a*) have shown in numerical simulations of a baroclinic two-layer model, that Rossby waves emerging from baroclinic instability of the mean flow become secondarily unstable when they reach a finite amplitude. They then feed energy directly to the streamwise flow along the lines of modulational instability.

The findings of Huang & Robinson (1998) are the basis of the third approach, pursued in SSST. SSST proposes an eddy-mean flow interaction mechanism for

https://doi.org/10.1017/jfm.2011.228 Published online by Cambridge University Press

mean flow emergence and persistence. The eddy mean flow interaction, can be well approximated using a stochastic turbulence model (STM). In the STM, the eddies draw most of their energy from the mean flow while the eddy excitation is represented as stochastic forcing (Farrell & Ioannou 1993*a*, *b*, *c*; DelSole & Farrell 1996; Newman, Sardeshmukh & Penland 1997; DelSole 2004). The stochastic forcing may represent excitation by external processes such as convection (as in the case of the Jovian jets or in the rotating tank experiments of Read *et al.* 2004) or it may additionally represent a parameterization of the nonlinear eddy-eddy interactions. As a result, the STM is a Langevin model of turbulence derived from the linearized Navier–Stokes equations in the spirit of rapid distortion theory (Hunt & Corruthers 1990). The advantage of the STM is that it provides a closure that determines a Gaussian approximation to the eddy statistics for any given mean flow. Its accuracy was extensively verified with fully nonlinear numerical studies of the eddy statistics in quasi-geostrophic turbulence (DelSole 1996, 2004; DelSole & Farrell 1996; Whitaker & Sardeshmukh 1998; Zhang & Held 1999) and has also been used to explain the turbulent structure in laboratory channel flows (Farrell & Ioannou 1993 *c*, 1998; Bamieh & Dahleh 2001; Jovanovic & Bamieh 2005; Hwang & Cossu 2010). Finally, this approximation has been shown to accurately predict the coherent flow structures for both the resolved and the largest sub-grid scales in three-dimensional turbulence under even homogeneous and isotropic conditions (Laval, Dubrulle & McWilliams 2003). The amplitude of the stochastic forcing will be taken as constant in this work. While for extrinsic sources of turbulence this is probably a good assumption, it is a crude assumption when the eddy excitation represents the nonlinear scattering to other scales, because its amplitude depends then on the very presence of the eddies. Progress on this problem has been made (DelSole 2001; Farrell & Ioannou 2009*c*) and while being an attractive avenue for future study, such a closure is not necessary for understanding the basic dynamics underlying the structural instability of the resulting equilibria.

In the context of SSST, the average eddy statistics provided by the STM are combined with the evolution equation for the mean flow to form an autonomous nonlinear system governing the joint evolution of the mean flow and the associated eddy statistics. The fixed points of this system represent steady mean flows in equilibrium with the mean eddy forcing and dissipation. The instability of these equilibria which brings about structural reconfiguration of the mean flow and the eddy statistics can then be studied. Using these methods, the structural instability of the joint eddy-mean flow equilibria have already been studied in barotropic and baroclinic rotating atmospheres (Farrell & Ioannou 2007, 2008, 2009*a*; Bernstein & Farrell 2010), and in the case of poloidal flow formation in tokamaks by drift wave turbulence (Farrell & Ioannou 2009*b*).

In this work, we investigate within the framework of SSST the role of the eddy mean flow feedbacks in the instability of the eddy-mean flow system equilibria giving rise to a mean flow. That is, we will focus on the mechanisms underlying the organization of the eddies by mean flow variations to produce Reynolds stresses that amplify these variations and eventually lead to an emerging jet. This paper is organized as follows. In § 2, we describe the evolution equations for the eddy-mean flow coupled system. In § 3, we calculate the eigenvalues of the linear operator governing the stability of the eddy-mean flow equilibria. In § 4, we elaborate on the role of the eddy-mean flow feedbacks and discuss the characteristics of the emerging jet in § 5. Sensitivity of the obtained results to changes in the eddy forcing and dissipation, is examined in § 6. We finally end with a brief discussion of the obtained results in § 7 and our conclusions in § 8.

https://doi.org/10.1017/jfm.2011.228 Published online by Cambridge University Press

2. Evolution equations for a barotropic flow

Consider a forced incompressible, planar flow confined in a channel ($-\infty < x < \infty$ and $0 \leqslant y \leqslant 2\pi$) on which we impose periodic boundary conditions at $y = 0$ and $y = 2\pi$. A streamfunction ψ can be defined such that: $[u, v] = [-\psi_y, \psi_x]$, where u, v are the streamwise, x, and cross-stream, y, components of velocity. The streamfunction evolves as

$$\partial_t \Delta\psi + J(\psi, \Delta\psi) = -r\Delta\psi + \nu\Delta^2\psi + F_{ext}, \tag{2.1}$$

where $\Delta = \partial^2_{xx} + \partial^2_{yy}$, is the Laplacian, $J(A, B) = A_x B_y - A_y B_x$ is the Jacobian operator, r, ν are the coefficients of linear and diffusive dissipation and F_{ext} is the external forcing. The forcing is required in two-dimensional studies of turbulent flows to sustain a statistical steady state. It represents either the actual excitation (for example, stirring by overturning convective systems in giant gas planets) or parameterizes missing three-dimensional processes (such as three-dimensional instabilities) cascading energy from three-dimensional (baroclinic) to planar (barotropic) flows. We decompose the streamfunction into a streamwise mean component (indicated with upper case) and an eddy component (indicated with primed quantities)

$$\psi(x, y, t) = \Psi(y, t) + \psi'(x, y, t), \tag{2.2}$$

and assume a vanishing external excitation for the mean flow. Under this decomposition and taking a streamwise mean (denoted by an overbar) of (2.1) yields the streamwise averaged equation for the x component of the mean velocity $\boldsymbol{U} = -\boldsymbol{\Psi}_y$

$$\partial_t \boldsymbol{U} = -\partial_y \overline{u'v'} - r\boldsymbol{U} + \nu \boldsymbol{U}_{yy}. \tag{2.3}$$

We then subtract (2.3) from (2.1) to obtain the evolution equation for the eddies

$$(\partial_t + \boldsymbol{U}\partial_x)\Delta\psi' - \psi'_x \boldsymbol{U}_{yy} = -r\Delta\psi' + \nu\Delta^2\psi' + (F_{ext} + F_e), \tag{2.4}$$

where

$$F_e = \overline{J(\psi', \Delta\psi')} - J(\psi', \Delta\psi'), \tag{2.5}$$

is the forcing term from the eddy–eddy interactions. Following previous studies of stochastic turbulence modelling (Farrell & Ioannou 1993*a*, *b*, 1994, 1995, 1996, 1998; DelSole & Farrell 1995, 1996; DelSole 1996, 1999, 2001, 2004), the eddy forcing term $F_{ext} + F_e$ is represented as a stochastic process. Under this assumption and taking harmonic perturbations of the form $\psi'(x, y, t) = \psi(y, t)\,\mathrm{e}^{\mathrm{i}kx}$, the Laplacian becomes $\Delta = D^2 - k^2$, where $D^2 = \partial^2/\partial y^2$, and the k Fourier component of vorticity $\boldsymbol{\omega} = \nabla^2\psi$ obeys the stochastic equation

$$(\partial_t + \mathrm{i}k\boldsymbol{U} + r)\boldsymbol{\omega} - \mathrm{i}k\boldsymbol{U}_{yy}\Delta^{-1}\boldsymbol{\omega} = \nu\Delta\boldsymbol{\omega} + F\xi(t). \tag{2.6}$$

Here, F and $\xi(t)$ are the spatial and temporal structure of the stochastic forcing, respectively, and Δ^{-1} the inverse Laplacian. We will consider an eddy field concentrated at a single wavenumber k. We will show in the sequel that we lose no generality by assuming a monochromatic eddy field.

We discretize the differential operators with finite differences. The reason is that although a continuous version of the eddy-mean flow system can be derived, the matrix form of the equations allows the use of matrix calculus. This will be necessary for obtaining the properties of the dynamics of the covariance of the eddy field and will facilitate analytic progress. The operators then, become finite-dimensional matrix approximations of the continuous operators and the variables $\boldsymbol{\omega}$, $\boldsymbol{U}$ become column

https://doi.org/10.1017/jfm.2011.228 Published online by Cambridge University Press

vectors with elements the values of the variables at the grid points. In matrix notation, (2.6) takes the form

$$\frac{\mathrm{d}\boldsymbol{\omega}}{\mathrm{d}t} = \boldsymbol{A}(\boldsymbol{U})\boldsymbol{\omega} + \boldsymbol{F}\boldsymbol{\xi}(t), \tag{2.7}$$

where the spatial structure of the forcing is given by the columns of the matrix $\boldsymbol{F}$ and $\boldsymbol{\xi}$ is a vector giving the time variation of the forcing. $\boldsymbol{A}$ is the matrix form of the linear dynamics about the mean flow $\boldsymbol{U}$ given by

$$\boldsymbol{A}(\boldsymbol{U}) = -\mathrm{i}k\ \mathrm{diag}(\boldsymbol{U})\ -\ \mathrm{i}k\ \mathrm{diag}(-D^2\boldsymbol{U})\Delta^{-1} - r\boldsymbol{I} + \nu\Delta, \tag{2.8}$$

where $\boldsymbol{I}$ is the identity matrix and diag$(\bullet)$ denotes the diagonal matrix with diagonal elements the vector $(\bullet)$. The linear dynamics comprises advection of perturbation vorticity by the mean flow, advection of the mean vorticity gradient $-D^2\boldsymbol{U}$ by the perturbations and dissipation.

Similarly, (2.3) is written as

$$\frac{\mathrm{d}\boldsymbol{U}}{\mathrm{d}t} = \boldsymbol{R} - r\boldsymbol{U} + \nu\boldsymbol{D}^2\boldsymbol{U}, \tag{2.9}$$

where

$$\boldsymbol{R} = -\partial_y\overline{u'v'} = -\frac{k}{2}\mathrm{vecd}[\mathrm{Im}(\Delta^{-1}\boldsymbol{\omega}\boldsymbol{\omega}^\dagger)], \tag{2.10}$$

is the Reynolds stress divergence expressed in terms of the streamwise mean enstrophy covariance matrix of the eddy field, $\boldsymbol{\omega}\boldsymbol{\omega}^\dagger$, $\dagger$ denotes the Hermitian transpose and vecd denotes the operation of extracting the diagonal elements of a matrix.

The random vector process $\boldsymbol{\xi}$ has statistically independent elements and is a Gaussian white noise in time with zero mean and unit variance so that

$$\langle\boldsymbol{\xi}\rangle = 0, \quad \langle\boldsymbol{\xi}\boldsymbol{\xi}^\dagger\rangle = \boldsymbol{I}\delta(t-s), \tag{2.11}$$

where the angle brackets denote an ensemble average over realizations of the forcing. The spatial localization of the excitation is dictated by the matrix $\boldsymbol{F}$ which is chosen to have elements

$$F_{ij} = \mathrm{e}^{-(y_i-y_j)^2/\delta^2}. \tag{2.12}$$

This specification leads to a statistically homogeneous excitation of the channel with forcing that is coherent over a distance δ. Finally, the forcing is normalized so that the variance level is a fraction ϵ of the energy of a constant mean flow with unit velocity. This normalization stems from the fact that typically the eddy variance is a fraction of the mean flow energy.

The system (2.7), (2.9) describes the dynamics of a single realization of the stochastically excited wave field interacting with the mean flow. Assuming a large number of independent realizations of the forcing and taking an ensemble average of the excited wave fields, we obtain a deterministic equation governing the evolution of the ensemble average enstrophy covariance matrix $\boldsymbol{C} = \langle\boldsymbol{\omega}\boldsymbol{\omega}^\dagger\rangle$

$$\frac{\mathrm{d}\boldsymbol{C}}{\mathrm{d}t} = \boldsymbol{A}(\boldsymbol{U})\boldsymbol{C} + \boldsymbol{C}\boldsymbol{A}^\dagger(\boldsymbol{U}) + \epsilon\boldsymbol{Q}, \tag{2.13}$$

where $\boldsymbol{Q} = \boldsymbol{F}\boldsymbol{F}^\dagger$ (Farrell & Ioannou 2003). Under an ergodic assumption, the ensemble average of the eddy Reynolds stress is equal to the streamwise average Reynolds stress, i.e. $\overline{u'v'} = \langle u'v'\rangle$. The mean flow therefore evolves as

$$\frac{\mathrm{d}\boldsymbol{U}}{\mathrm{d}t} = \boldsymbol{R}(\boldsymbol{C}) - r\boldsymbol{U} + \nu\boldsymbol{D}^2\boldsymbol{U}, \tag{2.14}$$

https://doi.org/10.1017/jfm.2011.228 Published online by Cambridge University Press

where

$$\boldsymbol{R}(\boldsymbol{C}) = -\frac{k}{2}\mathrm{vecd}[\mathrm{Im}(\Delta^{-1}\boldsymbol{C})], \tag{2.15}$$

is the average Reynolds stress divergence due to the eddy field at wavenumber k. Equations (2.13) and (2.14) form a deterministic, autonomous, globally stable nonlinear system for the evolution of the mean flow under the influence of its consistent field of eddies at wavenumber k. The attractor of this system may be a fixed point, a limit cycle or a chaotic attractor. Examples of each of these behaviours has been found in the SSST description of geophysical and plasma turbulence (Farrell & Ioannou 2003, 2008, 2009*b*). The fixed points $\boldsymbol{U}^E$ and $\boldsymbol{C}^E$, if they exist, satisfy simultaneously

$$\boldsymbol{A}(\boldsymbol{U}^E)\boldsymbol{C}^E + \boldsymbol{C}^E\boldsymbol{A}^\dagger(\boldsymbol{U}^E) = -\epsilon\boldsymbol{Q}, \quad \boldsymbol{R}(\boldsymbol{C}^E) = -r\boldsymbol{U}^E + \nu\boldsymbol{D}^2\boldsymbol{U}^E, \tag{2.16}$$

and these define statistical equilibria in the presence of an eddy field with covariance $\boldsymbol{C}^E$. The stability of the eddy-mean flow equilibria $\boldsymbol{U}^E$ and $\boldsymbol{C}^E$ can then be determined by considering the evolution of small perturbations $\delta\boldsymbol{U}$, $\delta\boldsymbol{C}$ about the equilibrium. Because of the operator Im in (2.15), we must write separate equations for the evolution of the real, $\delta\boldsymbol{C}^R$, and imaginary part, $\delta\boldsymbol{C}^I$, of the perturbation covariance. The resulting stability equations for the evolution of $\delta\boldsymbol{U}$, $\delta\boldsymbol{C}^R$ and $\delta\boldsymbol{C}^I$ can be written in the compact form as

$$\frac{\mathrm{d}}{\mathrm{d}t}\begin{pmatrix}\mathrm{vec}(\delta\boldsymbol{C}^R)\\ \mathrm{vec}(\delta\boldsymbol{C}^I)\\ \delta\boldsymbol{U}\end{pmatrix} = \boldsymbol{L}\begin{pmatrix}\mathrm{vec}(\delta\boldsymbol{C}^R)\\ \mathrm{vec}(\delta\boldsymbol{C}^I)\\ \delta\boldsymbol{U}\end{pmatrix}, \tag{2.17}$$

where vec is the vector representation of a matrix obtained by stacking sequentially the columns of a matrix on top of each other. As a result, $\mathrm{vec}(\delta\boldsymbol{C}^R)$ and $\mathrm{vec}(\delta\boldsymbol{C}^I)$ become $N^2 \times 1$ vectors for N discretization points in the channel and $\boldsymbol{L}$ is a $(2N^2 + N) \times (2N^2 + N)$ matrix. The structural stability operator $\boldsymbol{L}$ determines the stability of the eddy-mean flow equilibria.

It is worth noting that perturbation stability, determined by eigenanalysis of the operator $\boldsymbol{A}^E = \boldsymbol{A}(\boldsymbol{U}^E)$, does not necessarily imply structural stability, determined by eigenanalysis of the operator $\boldsymbol{L}$. If a mean flow is perturbation unstable, it is also structurally unstable. However, the converse is not true. In fact, it will be shown that the state of no mean flow, while perturbation stable in a dissipative fluid, is structurally unstable under sufficient forcing. The reason is that the non-zero eddy fluxes that are maintained by the forcing may induce mean flow changes that will, in turn, lead to increased fluxes resulting in a positive feedback and in instability of $\boldsymbol{L}$. It is this eddy-mean flow instability leading to the emergence of mean flows in a turbulent fluid that is addressed in this study. In the following sections, the diffusive eddy dissipation will initially be ignored and its effect on the jet forming instability will be considered in § 7.

3. The structural stability operator for a statistical equilibrium with no mean flow

Because a homogeneous eddy field in a constant flow cannot produce a Reynolds stress divergence $\boldsymbol{R}$, the state with no mean flow ($\boldsymbol{U}^E = 0$) and an eddy field with covariance

$$\boldsymbol{C}^E = \frac{\epsilon\boldsymbol{Q}}{2r}, \tag{3.1}$$

https://doi.org/10.1017/jfm.2011.228 Published online by Cambridge University Press

is a fixed point of the system (2.13)–(2.14). The goal is to determine the structural stability of this statistical equilibrium state that has no mean flow associated with it. The structural stability operator $\boldsymbol{L}$ of (2.17) takes in this case the form (see Appendix A for the derivation)

$$\boldsymbol{L} = \begin{pmatrix} -2r\boldsymbol{I}_{N^2} & 0 & 0 \\ 0 & -2r\boldsymbol{I}_{N^2} & \boldsymbol{L}^{IU} \\ 0 & \boldsymbol{L}^{UI} & -r\boldsymbol{I} \end{pmatrix}, \tag{3.2}$$

where $\boldsymbol{I}_{N^2}$ is the $N^2 \times N^2$ identity matrix. The operator $\boldsymbol{L}^{UI}$ determines the change in the Reynolds stress divergence, $\boldsymbol{R}$, due to a change in the eddy statistics $\delta\boldsymbol{C}$ and is given by

$$\boldsymbol{L}^{UI} = \frac{\partial \boldsymbol{R}}{\partial \delta \boldsymbol{C}} = -\frac{k}{2}\boldsymbol{J}(\boldsymbol{I} \otimes \Delta^{-1}), \tag{3.3}$$

where $\otimes$ denotes the Kronecker product defined in Appendix B and $\boldsymbol{J}$ is the $N \times N^2$ selection matrix given in Appendix A that extracts the diagonal elements of a matrix (see (A 7) and (A 10)). On the other hand, the operator $\boldsymbol{L}^{IU}$ determines the change in the eddy statistics $\delta\boldsymbol{C}$ due to the change in the mean flow $\delta\boldsymbol{U}$ and is given by:

$$\boldsymbol{L}^{IU} = -\frac{\epsilon k}{2r}\{\boldsymbol{Q} * \boldsymbol{I} - \boldsymbol{I} * \boldsymbol{Q} - [(\boldsymbol{Q}\Delta^{-1}) * \boldsymbol{I} - \boldsymbol{I} * (\boldsymbol{Q}\Delta^{-1})]\boldsymbol{D}^2\}, \tag{3.4}$$

where $*$ denotes the Khatri–Rao product defined in Appendix B.

From (3.2), we immediately see that the block-diagonal matrix $\boldsymbol{L}$ has N^2 eigenvalues $\lambda = -2r$ (from the upper block), with corresponding eigenvectors $[\delta\boldsymbol{C}^R, \delta\boldsymbol{C}^I, \delta\boldsymbol{U}] = [\boldsymbol{I}, 0, 0]$, representing decay of the perturbation covariance. In addition, because $\boldsymbol{L}^{UI}$ is an $N \times N^2$ matrix, the $N^2 - N$ vectors $[\delta\boldsymbol{C}^R, \delta\boldsymbol{C}^I, \delta\boldsymbol{U}] = [0, \boldsymbol{E}, 0]$, with $\boldsymbol{E}$ one of the $N^2 - N$ basis vectors of the nullspace of $\boldsymbol{L}^{UI}$ (cf. Appendix A), are eigenvectors of $\boldsymbol{L}$ with eigenvalue $\lambda = -2r$. As a result, $\boldsymbol{L}$ has a total of $2N^2 - N$ decaying eigenmodes with eigenvalue $-2r$ and $\delta\boldsymbol{U} = 0$ that do not modify the mean flow. The remaining $2N$ eigenvalues can be calculated by taking the time derivative of the equation corresponding to the third row in (2.17) and using the equation corresponding to the second row in (2.17) to obtain

$$\frac{\mathrm{d}^2\delta\boldsymbol{U}}{\mathrm{d}t^2} + 3r\frac{\mathrm{d}\delta\boldsymbol{U}}{\mathrm{d}t} + (2r^2\boldsymbol{I} - \boldsymbol{L}^{UI}\boldsymbol{L}^{IU})\delta\boldsymbol{U} = 0. \tag{3.5}$$

Looking for modal solutions of the form $\delta\boldsymbol{U} = \mathrm{e}^{\lambda_n t}\delta\boldsymbol{U}_n$ in (3.5) we obtain

$$\lambda_n = -\frac{3r}{2} \pm \frac{1}{2}\sqrt{r^2 + 4s_n}, \quad n = 1, \ldots, N, \tag{3.6}$$

where s_n are the N eigenvalues of the $N \times N$ matrix $\boldsymbol{S} = \boldsymbol{L}^{UI}\boldsymbol{L}^{IU}$. From (3.6) we obtain that the zero-mean flow equilibrium becomes unstable and mean flows emerge only if the eigenvalues of $\boldsymbol{S}$ are positive.

Matrix $\boldsymbol{S}$ determines the sensitivity of the Reynolds stress divergence to small changes in the mean flow in the quasi-static limit. That is, if we assume that the mean flow evolves slowly enough that it remains in equilibrium with the eddy covariance and satisfies at all times

$$\boldsymbol{A}(\boldsymbol{U})\boldsymbol{C} + \boldsymbol{C}\boldsymbol{A}^{\dagger}(\boldsymbol{U}) = -\epsilon\boldsymbol{Q}, \tag{3.7}$$

then the covariance perturbation becomes a function of the instantaneous mean flow perturbation. This $\delta\boldsymbol{C}(\delta\boldsymbol{U})$ is found by solving (3.7) linearized around the equilibrium

https://doi.org/10.1017/jfm.2011.228 Published online by Cambridge University Press

values or, equivalently, by solving $\mathrm{d}\delta\boldsymbol{C}/\mathrm{d}t = 0$. As a result, the change in the imaginary part of the covariance is in the notation of (3.2) given by

$$\mathrm{vec}(\delta\boldsymbol{C}^I) = (1/2r)\boldsymbol{L}^{IU}\delta\boldsymbol{U}. \tag{3.8}$$

In that approximation, the change in the Reynolds stress divergence induced by a change in $\delta\boldsymbol{U}$ is obtained by combining (3.3) with (3.8)

$$\delta\boldsymbol{R} = \frac{\partial\boldsymbol{R}}{\partial\delta\boldsymbol{C}^I}\mathrm{vec}(\delta\boldsymbol{C}^I) = \boldsymbol{L}^{UI}\boldsymbol{L}^{IU}\delta\boldsymbol{U} = \frac{1}{2r}\boldsymbol{S}\delta\boldsymbol{U}. \tag{3.9}$$

It is instructive to consider the predictions of mixing-length theory for the sensitivity operator $\boldsymbol{S}$. According to the mixing-length hypothesis, the eddy momentum flux is assumed proportional to the gradient of mean velocity $\overline{u'v'} = -\mu(\mathrm{d}\boldsymbol{U}/\mathrm{d}y)$, with $\mu > 0$, yielding a Reynolds stress divergence proportional to the curvature of the flow

$$\boldsymbol{R} = -\partial_y\overline{u'v'} = \mu\frac{\mathrm{d}^2\boldsymbol{U}}{\mathrm{d}y^2}. \tag{3.10}$$

So, $\boldsymbol{S}$ is the second derivative operator: $\boldsymbol{S} = \mu\boldsymbol{D}^2$ which has negative eigenvalues and acts as diffusion in the cross-stream direction. As a result, according to mixing-length theory, a state of zero-mean flow in the presence of an eddy field would always be structurally stable and no mean flows could emerge. In the next section, we show that, quite generally, $\boldsymbol{S}$ is the sum of two commuting operators. The first is a diffusion operator with negative coefficient of viscosity (anti-diffusion) and the other a diffusion or hyper-diffusion operator. We also show that the zero-mean flow can be rendered structurally unstable in the presence of homogeneously forced eddies.

It is also worth addressing the case of an eddy field that comprises a band of wavenumbers k. It can be readily shown that in this case, the eigenvalues of the structural stability operator are obtained by solving

$$\frac{\mathrm{d}^2\delta\boldsymbol{U}}{\mathrm{d}t^2} + 3r\frac{\mathrm{d}\delta\boldsymbol{U}}{\mathrm{d}t} + \left(2r^2\boldsymbol{I} - \sum_k \boldsymbol{S}_k\right)\delta\boldsymbol{U} = 0, \tag{3.11}$$

where $\boldsymbol{S}_k = \boldsymbol{L}_k^{UI}\boldsymbol{L}_k^{IU}$ is the sensitivity operator at each streamwise wavenumber k. Since $\boldsymbol{S}_k$ can be shown to commute, the eigenvalues of the structural stability operator are given in this case by

$$\lambda_n = -\frac{3r}{2} \pm \frac{1}{2}\sqrt{r^2 + 4\sum_k s_n(k)}, \quad n = 1, \ldots, N, \tag{3.12}$$

where $s_n(k)$ are the eigenvalues of $\boldsymbol{S}_k$. Note that this result pertains to the simplified case considered here. The same analysis on a β plane, or including diffusive dissipation (as treated in Appendix D), yields similar results only in the asymptotic limits of $\beta \ll 1$ and $\nu \ll 1$.

https://doi.org/10.1017/jfm.2011.228 Published online by Cambridge University Press

4. Eigenvalues of the Reynolds stress sensitivity operator for a statistical equilibrium with no mean flow

In Appendix A, it is shown that the sensitivity operator is the sum of two commuting operators

$$\boldsymbol{S} = \frac{\epsilon k^2}{4r}\left\{\underbrace{[\boldsymbol{Q}\circ\Delta^{-1} - \boldsymbol{I}\circ(\Delta^{-1}\boldsymbol{Q})]}_{\boldsymbol{S}^{ad}} - \underbrace{[\Delta^{-1}\circ(\boldsymbol{Q}\Delta^{-1}) - \boldsymbol{I}\circ(\Delta^{-1}\boldsymbol{Q}\Delta^{-1})]\boldsymbol{D}^2}_{\boldsymbol{S}^{vg}}\right\}, \tag{4.1}$$

where $\circ$ denotes the Hadamard product $(A\circ B)_{ij} = A_{ij}B_{ij}$. The first operator, $\boldsymbol{S}^{ad}$, determines the sensitivity of the Reynolds stress divergence to changes in the mean velocity advection. The second operator, $\boldsymbol{S}^{vg}$, determines the sensitivity of the Reynolds stress divergence to changes in the mean vorticity gradient. The commutation of these two operators as well as many of the properties that allow analytical progress, derive from the fact that all the matrices in (4.1) are real symmetric and circulant. This matrix property is defined in Appendix C and reflects the periodicity and the translational invariance in the cross-stream direction. Because the Hadamard product of symmetric and circulant matrices is also symmetric and circulant, both $\boldsymbol{S}^{ad}$ and $\boldsymbol{S}^{vg}$ are real symmetric and circulant, have real eigenvalues, s_n^{ad} and s_n^{vg} and eigenfunctions, the harmonic basis functions

$$\delta\boldsymbol{U}_n = \sin(n\boldsymbol{y}), \tag{4.2}$$

where $\boldsymbol{y}$ is the column vector with ith element the collocation point y_i, $i = 1, 2, \ldots, N$. The eigenvalues of $\boldsymbol{S}$ depend on the wavenumber n of the mean flow perturbation and are given by

$$s_n = \frac{\epsilon k^2}{4r}\left(s_n^{ad} - s_n^{vg}\right). \tag{4.3}$$

Both s_n^{ad} and s_n^{vg} are positive if the stochastic forcing is correlated (refer to Appendix C for a proof in the case of homogeneous, Gaussian-correlated stochastic forcing). Consequently, advection of the eddy vorticity by the perturbed flow is destabilizing, while advection of the perturbed mean vorticity gradient by the eddies has a stabilizing tendency.

The eigenvalues s_n^{ad} and s_n^{vg} were numerically calculated for $N = 401$ grid points for which the obtained results are resolved. Numerical convergence to the continuous system was verified by doubling the resolution. The computed eigenvalues are shown in figure 1 (dots) as a function of the wavenumber n of the mean flow for two values of the streamwise wavenumber of the eddy field k. Useful asymptotic expressions for the eigenvalues are obtained in the continuous limit ($N\to\infty$). If we define the scale of the eddy field as $l_e = \min(1/k, \delta)$, it is shown in Appendix C that for a mean flow perturbation with a small scale compared to the eddy scale ($nl_e \gg 1$)

$$s_n^{ad} \simeq 2, \quad s_n^{vg} \simeq c_1(k\delta)\frac{n^2}{k^2}, \tag{4.4}$$

where $c_1(k\delta)$ is given by (C 45). This implies that high mean flow wavenumbers have $s_n < 0$ and hence from (3.6) are structurally stable. In the more physically relevant regime, in which the scale of the mean flow perturbation is much larger than the eddy scale ($nl_e \ll 1$), it is shown in Appendix C that

$$s_n^{ad} \simeq \begin{cases} \delta^2 n^2, & \text{for } kl_c \ll 1, \\ c_2(k,\delta)n^2, & \text{for } kl_c \gg 1, \end{cases} \quad s_n^{vg} \simeq \begin{cases} 2n^2/k^2, & \text{for } kl_c \ll 1, \\ c_3(k\delta)n^4/k^4, & \text{for } kl_c \gg 1, \end{cases} \tag{4.5}$$

https://doi.org/10.1017/jfm.2011.228 Published online by Cambridge University Press

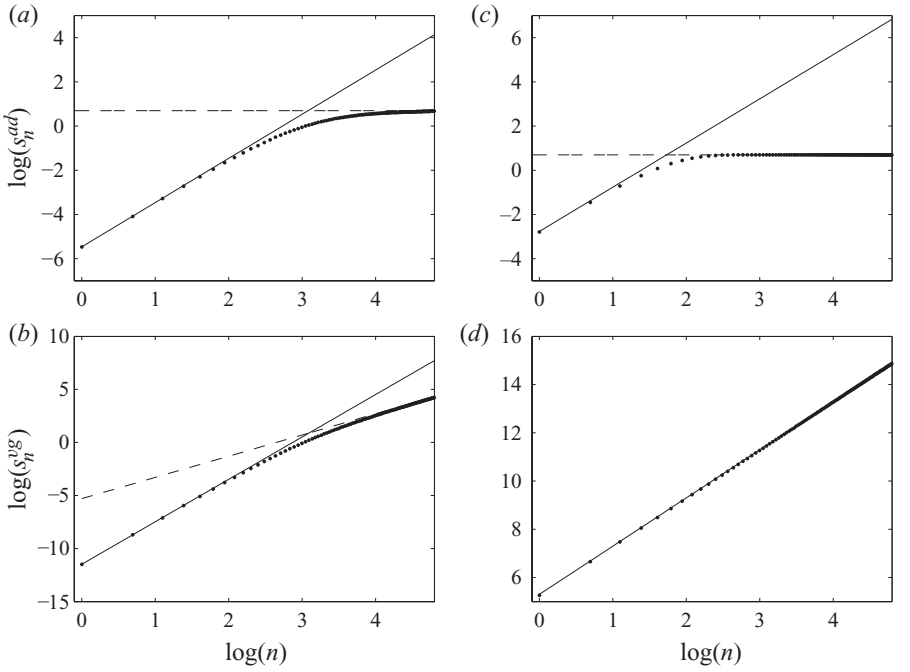


FIGURE 1. (*a*, *b*) The numerically calculated eigenvalues s_n^{ad} of $\boldsymbol{S}^{ad}$ (*a*) and s_n^{vg} of $\boldsymbol{S}^{vg}$ (*b*) as a function of the mean flow wavenumber n in the $kl_c \gg 1$ limit (dots). The analytically calculated limits for low n (solid line) and large n (dashed line), given by (4.4) and (4.5) are also plotted for reference. (*c*, *d*) The same as (*a*, *b*) but for $kl_c \ll 1$. The streamwise wavenumber is $k = 20$ for (*a*) and (*b*) and $k = 0.1$ for (*c*) and (*d*). For all panels $\delta = 0.25$.

where $l_c = 2\pi$ is the width of the channel and the constants c_2 and c_3 given in (C 30) and (C 31), respectively, depend only on k and on the scale δ of the forcing. The analytic results of (4.4)–(4.5) are also illustrated in figure 1, where we observe a very good agreement with the exact, numerical results. It can be readily seen from (4.5), that eddies with high wavenumber k potentially lead to structural instability and emergence of a mean flow with low wavenumber n, as then $s_n^{ad} > s_n^{vg}$. On the other hand, eddies with small k are unable to lead to jet formation. Therefore, there is a minimum value k_c for the eddies, below which all the eigenvalues s_n are negative and the Reynolds stress divergence relaxes all mean flow perturbations back to the equilibrium state. This minimum wavenumber is a function of the forcing correlation scale δ and behaves as (cf. Appendix C)

$$k_c \sim 1/\sqrt{\delta}, \tag{4.6}$$

for $\delta \ll 1$. As a result, for uncorrelated forcing for which $\delta \to 0$, the system is globally stable and no mean flows emerge. In the opposite limit of spatially correlated forcing ($\delta \to \infty$), the minimum wavenumber k_c becomes 1.

From the limiting behaviour of the eigenvalues for small n, we also see that advection of the eddy vorticity by the perturbed mean flow acts exactly as the anti-diffusion operator $-\tilde{\mu}\mathrm{d}^2/\mathrm{d}y^2$, with $\tilde{\mu}$ being a positive constant. For a forcing that excites eddies with smaller streamwise than spanwise scales ($k\delta \gg 1$), $c_2 l_e^2 \simeq 2/k^2$ and the diffusion coefficient $\tilde{\mu}(\epsilon, r, k, \delta)$ approaches a value that is independent of the

https://doi.org/10.1017/jfm.2011.228 Published online by Cambridge University Press

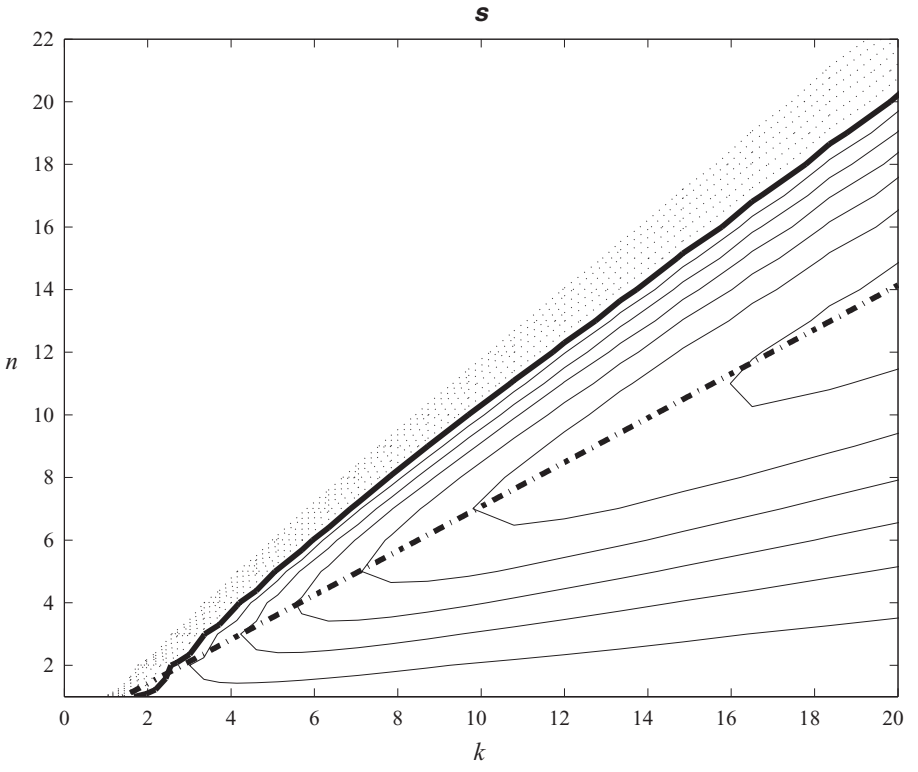


FIGURE 2. Contours of the numerically calculated eigenvalues s_n of the Reynolds stress sensitivity operator $\boldsymbol{S}$, as a function of the mean flow wavenumber n and the streamwise wavenumber k of the eddy field. The eigenvalues are divided by k^2 for each wavenumber for illustration purposes. The contour interval is 0.05, positive and negative values are shown by the solid and dashed lines, respectively, and the zero contour is shown by the thick solid line. Note that the contours are slightly jagged due to the fact that the values of n are discrete. The mean flow wavenumber n_{max} that corresponds to the largest eigenvalue and is given by (4.8), is also shown (thick dash dotted line) for reference. The values of ϵ, r influence only the values and not the form of the contours (here $\epsilon/r = 4$). The value of δ will influence the position of the zero contour line as discussed in the text (here $\delta = 0.25$).

spatial properties of the forcing, i.e.,

$$\tilde{\mu} \simeq \epsilon/2r. \tag{4.7}$$

On the other hand, advection of the perturbed mean vorticity gradient by the eddies acts as a hyper-diffusion operator for large streamwise wavenumbers, k, and as a diffusion operator for low k with the same diffusion coefficient $\tilde{\mu}$ in the limit of $k\delta \gg 1$.

Contours of the numerically calculated eigenvalues of $\boldsymbol{S}$ are plotted in figure 2 as a function of the mean flow wavenumber n and the streamwise wavenumber of the eddy field k. As the streamwise wavenumber of the eddies increases, there is a larger number of eigenstructures for which the equilibrium state is potentially structurally unstable (i.e., $s_n > 0$), and the maximum eigenvalues occur at larger values of n. The mean flow wavenumber n that produces the largest Reynolds stress sensitivity (jet forming stress) is readily shown from (4.5) in the limit of $k\delta \gg 1$ to be at

$$n_{max} = k/\sqrt{2}, \tag{4.8}$$

https://doi.org/10.1017/jfm.2011.228 Published online by Cambridge University Press

yielding a maximum eigenvalue $s_n = \epsilon k^2/8r$. The maximum mean flow wavenumber given by (4.8) is also shown in figure 2, where we can see a good agreement with the exact numerical results.

5. Instability characteristics

From (3.6), we can see that the structural stability of the state with no mean flow depends on the eddy dissipation r and the sensitivity of the Reynolds stress divergence as measured by s_n. Two necessary conditions are required for instability to occur. The first condition is that s_n should be positive for a mean flow perturbation with wavenumber n. That is, instability occurs only when the Reynolds stress divergence tends to reinforce the mean flow perturbation. As discussed in § 4, this condition is met when the streamwise wavenumber k is above the minimum wavenumber k_c. The second condition is that the forcing variance ϵ should be above a certain threshold, so that the eddy forcing can overcome the mean flow dissipation. By solving (3.6) for the neutral stability condition $\lambda_n = 0$ and using (4.3), we obtain that for a mean flow perturbation with a given wavenumber n, this threshold is

$$\epsilon_c = \frac{8r^3}{k^2\left(s_n^{ad} - s_n^{vg}\right)}. \tag{5.1}$$

The minimum input variance $\epsilon_{min} = \min_n(\epsilon_c)$ that is required to give rise to a mean flow with any wavenumber n is given as the threshold for the wavenumber n for which we have the maximum stress sensitivity (maximum $s_n^{ad} - s_n^{vg}$). Figure 3 illustrates the minimum input variance as a function of k. We observe that the minimum forcing amplitude drops rapidly with k, showing that forcing at larger streamwise wavenumbers is more efficient, as less eddy variance is needed to give rise to mean flows.

When the two necessary conditions are met, i.e., when $k > k_c$ and $\epsilon > \epsilon_{min}$, there is a number of emerging jets, whose mean velocity along with the corresponding Reynolds stress divergence grow exponentially. The numerically calculated eigenvalues λ_n for a given forcing strength are shown in figure 4(a) as a function of n for two streamwise wavenumbers. As k increases, there is a larger number of unstable jet structures and the maximum growth rate is attained at larger mean flow wavenumbers. Figure 4(b) shows the most unstable mean flow perturbation, when $k = 10$ along with the corresponding Reynolds stress divergence. We observe that the stress divergence is in phase with the mean flow perturbation and reinforces it. Therefore, both grow exponentially without any translation in y. The maximum growth rate as a function of k is shown in figure 4(c) for a given eddy dissipation. The maximum growth rate is proportional to the streamwise wavenumber k and also grows roughly as the square root of the forcing strength for large values of ϵ (not shown). The linear dependence on k can be traced to the fact that the maximum stress sensitivity is $s_n = (\epsilon k^2/8r)$ (cf. § 4) leading to a k^2 factor within the square root in (3.6) that dominates the growth rate for large wavenumbers. We also observe that the growth rate increases with the correlation scale δ, as the instability appears at lower streamwise wavenumbers. However, the slope of the maximum growth rate with k is insensitive to the choice of δ (cf. section 6.2 for further discussion). The mean flow wavenumber n of the jet that corresponds to the most unstable eigenvalue is plotted in figure 4(d) as a function of k. We observe that the width of the most unstable structure is proportional to the

https://doi.org/10.1017/jfm.2011.228 Published online by Cambridge University Press

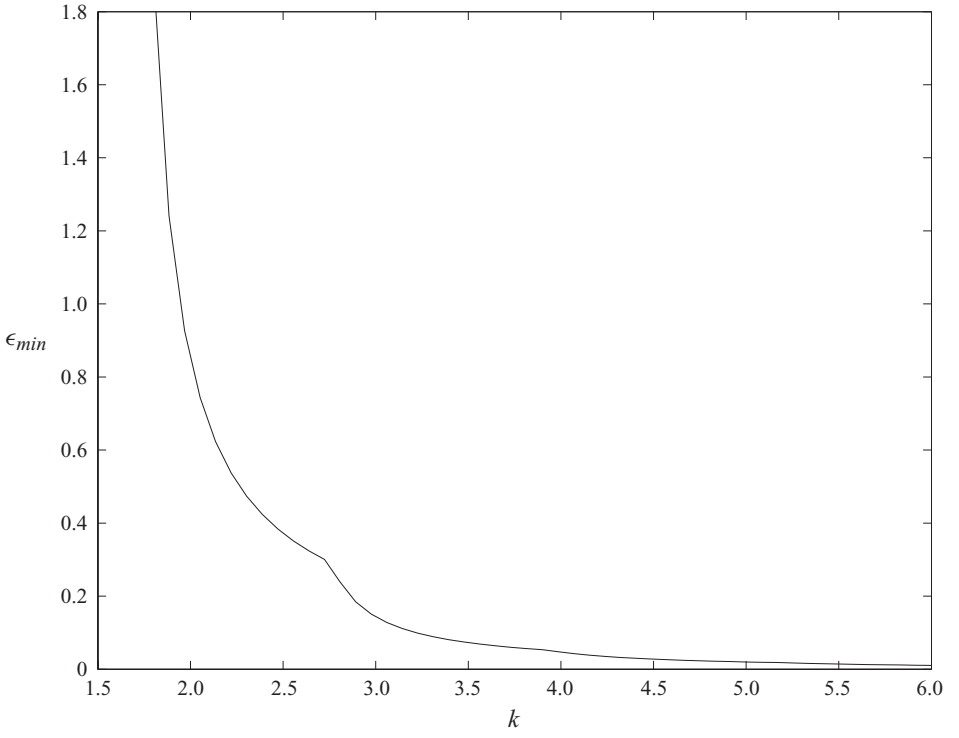


FIGURE 3. Minimum input variance ϵ_{min} as a function of streamwise wavenumber k for $r=0.2$ and $\delta=0.25$. The minimum ϵ_{min} is calculated by numerically finding the minimum of (5.1) or, equivalently, the maximum of $s_n^{ad}-s_n^{vg}$ over all n. The kink observed near $k=3$ as well as two others near $k=4$ and $k=5$ that are not evident, are due to the fact that the minimum corresponds to a different mean flow wavenumber n before and after the kink.

horizontal wavelength of the forcing as the mean flow wavenumber for which the maximum fluxes are attained is proportional to k (cf. (4.8)).

6. Sensitivity tests

In the previous sections, we studied the structural stability of the flow with zero mean velocity and the underlying mechanisms, when the damping was linear and the forcing was homogeneous and Gaussian correlated in vorticity. Sensitivity studies, changing the above assumptions, are presented in this section.

6.1. *Influence of diffusive dissipation*

We first discuss the sensitivity of the obtained results to a change in the type of dissipation. The SSST system in the presence of diffusive dissipation is formulated in Appendix D. The structural stability of the zero mean flow is shown to be governed in the limit of small diffusion ($\nu \ll 1$) by the Reynolds stress sensitivity operator $\boldsymbol{S}^v$ that is given by the expression

$$\boldsymbol{S}^v = \frac{\epsilon k^2}{4}\left\{\underbrace{[\boldsymbol{I}\circ(\boldsymbol{Q}\Delta^{-2})-\Delta^{-1}\circ(\Delta^{-1}\boldsymbol{Q})]}_{\boldsymbol{S}^{adv}}-\underbrace{[\boldsymbol{I}\circ(\Delta^{-2}\boldsymbol{Q}\Delta^{-1})-\Delta^{-1}\circ(\Delta^{-1}\boldsymbol{Q}\Delta^{-1})]\boldsymbol{D}^2}_{\boldsymbol{S}^{vgv}}\right\}. \tag{6.1}$$

https://doi.org/10.1017/jfm.2011.228 Published online by Cambridge University Press

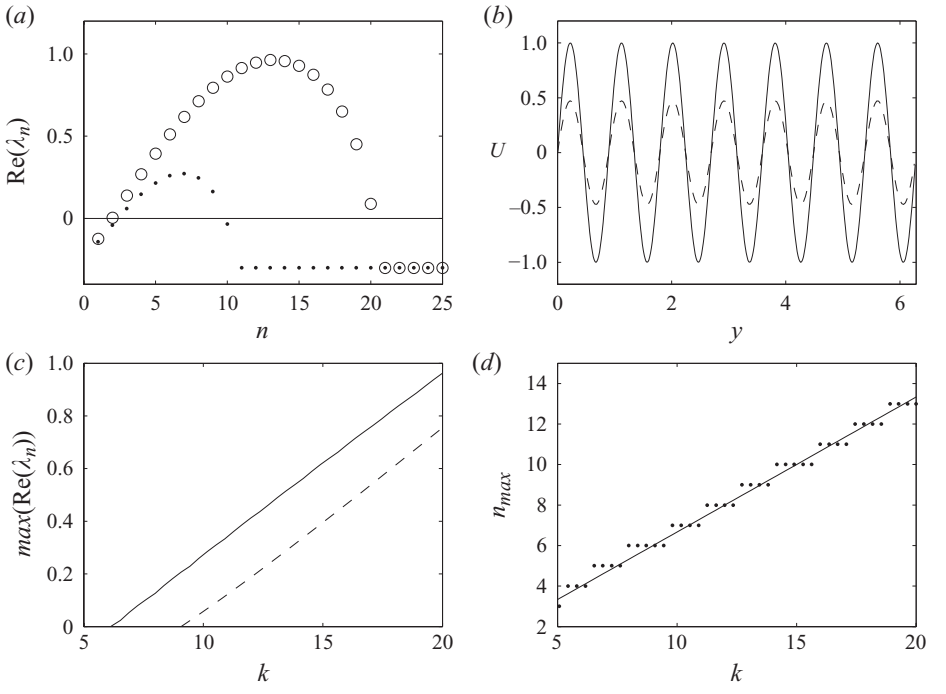


FIGURE 4. (*a*) Real part of the numerically calculated eigenvalues λ_n of the structural stability operator $\boldsymbol{L}$ as a function of mean flow wavenumber n for $k=10$ (dots) and $k=15$ (circles). (*b*) The most unstable mean flow perturbation (solid line) and the corresponding Reynolds stress divergence (dashed line) for $k=10$. (*c*) Maximum growth rate as a function of streamwise wavenumber k for $\delta=0.25$ (solid line) and $\delta=0.1$ (dashed line). (*d*) Mean flow wavenumber n for the most unstable eigenfunction (dots), as a function of k. A line of slope 2/3 is also plotted for reference (solid line). For all subparts, $r=0.2$, $\delta=0.25$ and the input variance is $\epsilon=0.01$.

Again, the two terms $\boldsymbol{S}^{adv}$ and $\boldsymbol{S}^{vgv}$ commute and determine the sensitivity of the Reynolds stress divergence to changes in the mean velocity advection and to changes in the mean vorticity gradient, respectively. Both are real symmetric circulant matrices with positive eigenvalues and the eigenvalues of $\boldsymbol{S}^{v}$ are consequently given by: $s_n^v=(\epsilon k^2/4)(s_n^{adv}-s_n^{vgv})$. The eigenvalues s_n^{adv} and s_n^{vgv} were numerically calculated for $N=401$ grid points and are illustrated in figure 5 as a function of mean flow wavenumber n. Comparison to figure 1 shows the same qualitative behaviour of the eigenvalues as determined by (4.4)–(4.5). The eigenvalues appear to be closely approximated by $s^{adv}\simeq s^{ad}/k^2$ and $s^{vgv}\simeq s^{vg}/k^2$ in the limits of validity of (4.4)–(4.5). The reason is that the equilibrium eddy covariance is proportional to $\Delta^{-1}\boldsymbol{Q}$ instead of $\boldsymbol{Q}$, adding roughly an additional $1/k^2$ factor to the eigenvalues. As a result, the eddy-mean flow feedbacks underlying the structural instability of the statistical equilibrium with no mean flow do not depend qualitatively on the details of the type of dissipation.

The eigenvalues of the structural stability operator $\boldsymbol{L}$ are calculated in Appendix D. For low values of diffusion ν, an approximate expression for λ_n in terms of s_n^v was also derived (see (D 6) and (D 7)). Comparison of numerically calculated eigenvalues and those derived from (D 6) and (D 7) showed a very good agreement for $\nu=10^{-3}$. Figure 6(*a*) shows the calculated eigenvalues λ_n as a function of n for this value

https://doi.org/10.1017/jfm.2011.228 Published online by Cambridge University Press

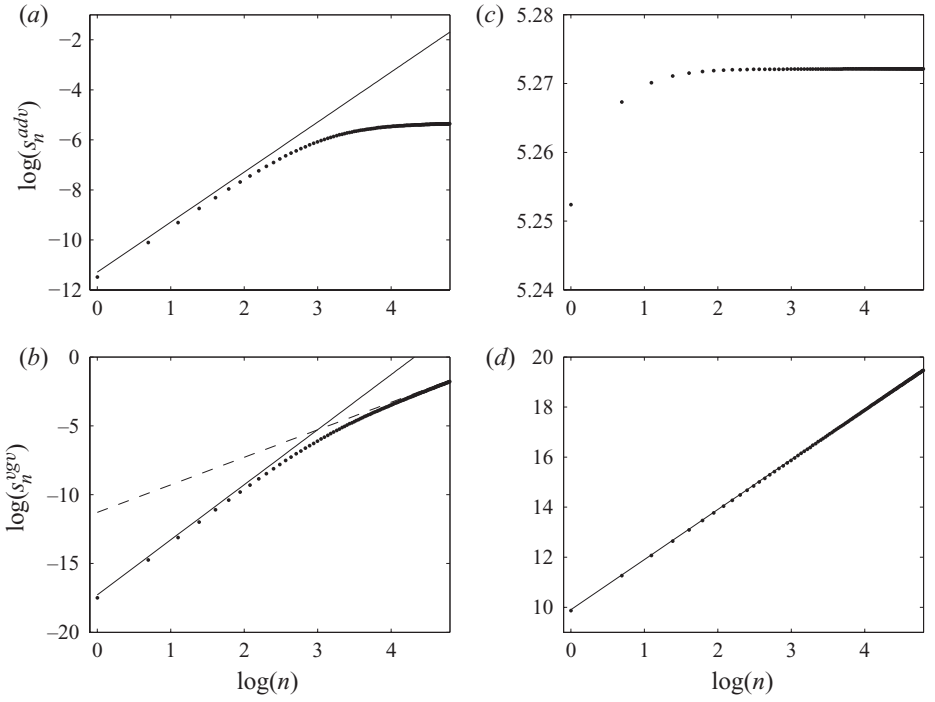


FIGURE 5. (*a*, *b*) Eigenvalues s_n^{adv} of $\boldsymbol{S}^{adv}$ (dots in *a*) and s_n^{vgv} of $\boldsymbol{S}^{vgv}$ (dots in *b*) as a function of mean flow wavenumber n in the $kl_c \gg 1$ regime. Straight lines with slope 2 (solid line) and with slope 4 (dashed line) are also plotted for reference. (*c*, *d*) The same as (*a*), (*b*) but for the $kl_c \ll 1$ regime. For subparts (*a*), (*b*), $k = 20$ and for (*c*) and (*d*) $k = 0.1$. For all panels $\delta = 0.25$.

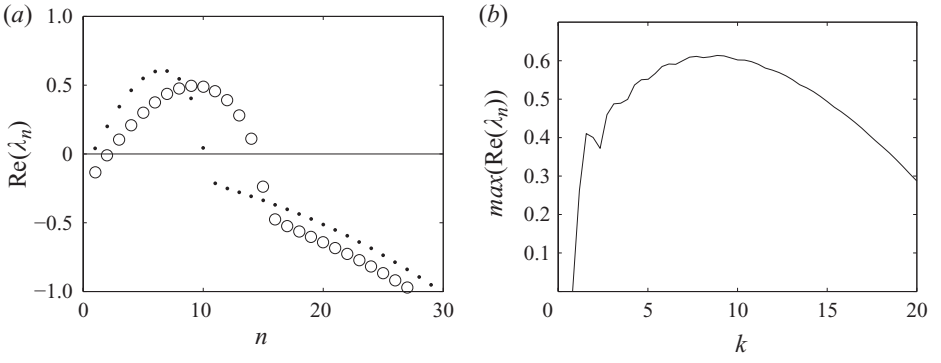


FIGURE 6. (*a*) Real part of the eigenvalues λ_n of the structural stability operator $\boldsymbol{L}$ as a function of mean flow wavenumber n for $k = 10$ (dots) and $k = 15$ (circles). (*b*) Maximum growth rate as a function of streamwise wavenumber. For both panels $\nu = 10^{-3}$, $\epsilon = 0.01$ and $\delta = 0.25$.

of diffusion coefficient. Again, the two necessary conditions for instability, that is $k > k_c$ and $\epsilon > \epsilon_{min}$ hold in this case as well. The critical minimum input variance ϵ_{min} required for structural instability is approximately

$$\epsilon_{min} \sim \frac{\nu^3}{k^2} + O(\nu^4), \tag{6.2}$$

https://doi.org/10.1017/jfm.2011.228 Published online by Cambridge University Press

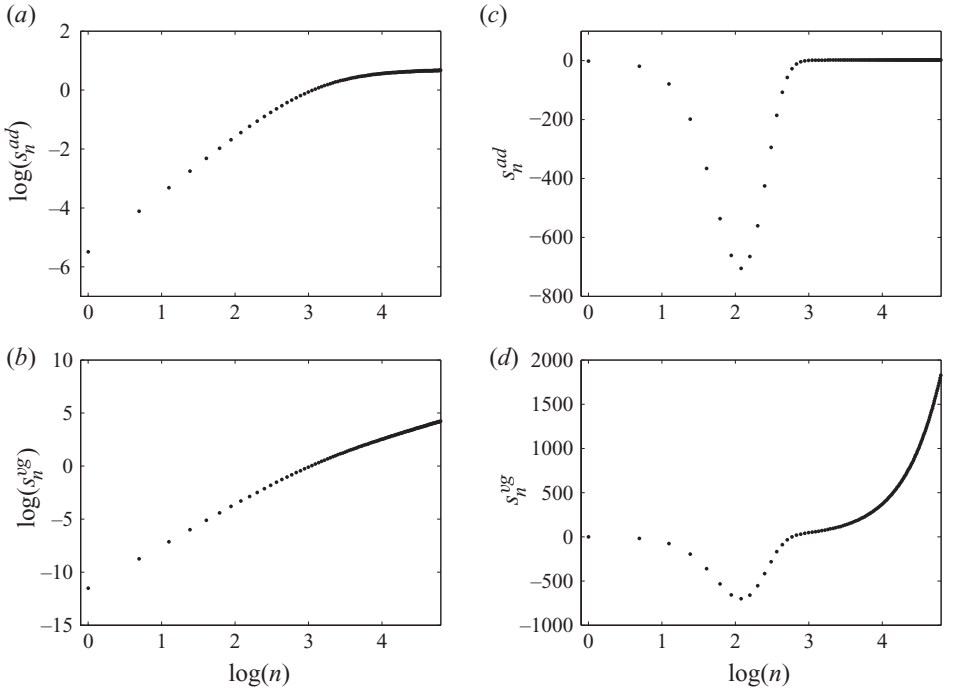


FIGURE 7. (*a*, *b*) Eigenvalues s_n^{ad} of $\boldsymbol{S}^{ad}$ (dots in *a*) and s_n^{vg} of $\boldsymbol{S}^{vg}$ (dots in *b*) as a function of mean flow wavenumber n in the $kl_c \gg 1$ regime. (*c*, *d*) The same as (*a*, *b*) but for the $kl_c \ll 1$ regime. For (*a*) and (*b*), $k = 20$ and for (*c*) and (*d*), $k = 0.1$. the forcing covariance is given by $\boldsymbol{Q}_v$ and $\delta = 0.25$.

for large streamwise wavenumbers. The growth rate of the structural instability is plotted in figure 6(*b*). Since diffusive dissipation increases quadratically with wavenumber, the maximum growth rate is bounded for large k, unlike the case of linear damping. Finally, the width of the emerging jet is proportional to the horizontal wavelength of the forcing, or equivalently the wavenumber n_{max} of the jet corresponding to the most unstable eigenvalue is proportional to the streamwise wavenumber k (not shown).

6.2. *Influence of the forcing characteristics*

We are interested in exploring the sensitivity of the structural instability to the structure of the forcing. We take the forcing covariance to be either $\boldsymbol{Q}_v = \Delta^{-1}\boldsymbol{Q}\Delta^{-1}$, or $\boldsymbol{Q}_e = M^{-1/2}\boldsymbol{Q}M$, where M is the energy metric given by (C 16) and $\boldsymbol{Q}$ is the forcing covariance matrix with the characteristics defined in § 2. The first choice, $\boldsymbol{Q}_v$, corresponds to a stochastic excitation of cross-stream velocity with the same spatial and temporal correlation as in the vorticity forcing case. With the second choice, $\boldsymbol{Q}_e$, we excite the system so that there is a Gaussian correlation in energy, rather than in vorticity. Therefore, an uncorrelated forcing would correspond in this case to each degree of freedom receiving equal energy.

The eigenvalues of the stress sensitivity operator $\boldsymbol{S}$, as well as $\boldsymbol{S}^{ad}$ and $\boldsymbol{S}^{vg}$ were numerically calculated for each of the two cases. Figure 7 shows the eigenvalues s_n^{ad} (figure 7*a*, *c*) and s_n^{vg} (figure 7*b*, *d*) as a function of mean flow wavenumber n for the case of $\boldsymbol{Q}_v$. Similar results are obtained for $\boldsymbol{Q}_e$ and are not shown.

https://doi.org/10.1017/jfm.2011.228 Published online by Cambridge University Press

Comparison of figures 7 (*a*) and (*b*) and 1 (*a*) and (*b*), show that for large streamwise wavenumbers, the results of §3 are insensitive to the choice of forcing covariance. However, figure 7 (*c*) and (*d*) illustrates that for smaller values of k, advection of the eddy vorticity produces a Reynolds stress divergence that is stabilizing and advection of the perturbed mean vorticity gradient by the eddies produces a Reynolds stress divergence that is destabilizing. As a result, we expect that the minimum wavenumber k_c, below which the flow is necessarily structurally stable ($s_n < 0$) to be larger in this case. This minimum wavenumber was empirically found to be $k_c \sim 1/\delta$ for $\boldsymbol{Q}_v$, with a slightly different dependence for $\boldsymbol{Q}_e$. Consequently, for a given correlation scale δ, forcing with smaller cross-stream scales is required to form a streamwise jet. In addition, no jets emerge in the limit $\delta -> 0$ when the forcing is uncorrelated, regardless of the details of the forcing.

7. Discussion

We now summarize the main results of this work and compare them to other observational and modelling studies. In this study, the initial structural instability of a zero mean flow under homogeneous forcing that leads to the emergence of streamwise jets was addressed. The basic assumption was that the interaction of the eddies with the mean flow is non-local in wavenumber space and that the eddy excitation can be modelled by a random process. First of all, we showed that advection of the eddy vorticity by the infinitesimal mean flow, that is shearing of the eddies, is the jet forming mechanism. This result is in agreement with previous numerical studies (Nozawa & Yoden 1997; Huang & Robinson 1998; Salyk *et al.* 2006; Kitamura & Ishioka 2007), which found that shearing of the eddies intensifies or sustains the mean flow. We also showed that the jets emerge when the forcing excites scales smaller than a certain minimum scale and when the forcing amplitude is above a certain threshold. When these two conditions are met, the eddy-mean flow system is structurally unstable. Investigation of the structural instability revealed that the wavenumber of the most unstable mean flow perturbation is of the same order as the streamwise wavenumber k of the most energetic eddies and the growth rate increases linearly with this k. This in agreement with Kitamura & Ishioka (2007), who found that forcing at small scales is necessary for jet formation as the eddies having small scales have the most significant contribution to momentum flux convergence.

However, it should be noted that neither the appearance of the initial instability guarantees the existence of a steady finite-amplitude jet, nor the scale of the emerging infinitesimal mean flow necessarily coincides with the scale of the finite-amplitude jet if this exists. Addressing this problem requires the study of the equilibration of the structural instability. Previous studies following the SSST approach (Farrell & Ioannou 2003, 2007, 2008, 2009*a*), have shown that a finite-amplitude jet may not be steady, as the non-linear eddy-mean flow system has also periodic solutions or a chaotic attractor. It was also shown in these studies that in addition to structural stability, perturbation stability also plays a crucial role in the evolution of the eddy-mean flow system. Therefore, rotation (the β effect) and the amount of eddy dissipation are key factors for the existence of steady solutions and the scale of the equilibrated jet, if such a solution exists. It was found that only in the case of marginal initial structural instability, the scale of the equilibrated jet coincides with the scale of the most unstable mean flow perturbation. In the case of stronger eddy forcing for which a stable equilibrium could be found, the most unstable perturbation predicted by this theory emerges initially. However, the resulting finite-amplitude jet

https://doi.org/10.1017/jfm.2011.228 Published online by Cambridge University Press

that corresponds to this scale is perturbation unstable and the jet readjusts, forming a perturbation stable jet with a smaller mean flow wavenumber. As a result, we typically under-predict the observed jet scale based only on the initial structural instability.

To illustrate this, we attempt to predict the spacing of the banded jets in Jupiter, using the results in this work. We non-dimensionalize the equations, choosing $L = 4000$ km and $T = 10$ h (the length of the Jovian day) as the length and time scales, respectively, and $V = L/T = 111$ ms^{-1} as the velocity time scale. The channel then corresponds to a typical mid-latitude portion of the Jovian atmosphere. We assume that the fluid is forced by convection. We therefore choose the de-correlation scale δ to be the scale of the convective storms, which is 1000 km (Ingersoll *et al.* 2000), corresponding to a non-dimensional $\delta = 0.25$. The amplitude of the forcing, as well as the damping parameters for Jupiter are not well known individually. What is known is the turbulent large-scale r.m.s. velocity, which is $O(5\text{ms}^{-1})$ (Salyk *et al.* 2006). We therefore adjust ϵ and r to produce the observed level of turbulence. We also assume that the eddy field comprises of a band of wavenumbers k with the largest wavenumber (non-dimensional $k = 400$) corresponding to the horizontal scale of convection. The eigenvalues of the structural stability operator are given in this case by (3.12). The eigenfunction with the largest growth rate was found in this case to have a non-dimensional mean flow wavenumber $n = 8$ corresponding to a scale of 3000 km. This is about a third of the observed jet spacing in the Jovian atmosphere, but as discussed above we expect that the adjustments occurring during its equilibration will increase its scale towards the observed one as shown in Farrell & Ioannou (2007).

A different approach from SSST that also assumes non-local interactions in wavenumber space is modulational instability (Gill 1974; Lorenz 1974; Connaughton *et al.* 2010), in which the jets appear as a result of modulational rather than structural instability. The width of the emergent jet, is the scale with the fastest growth of a purely streamwise (zonal) wave interacting non-linearly with three Rossby waves, one of which is assumed to be a purely cross-stream (meridional) wave. The wavenumber of the fastest growing zonal wave (i.e. the mean flow wavenumber), is proportional to the streamwise wavenumber of the primary meridional wave and the fastest growth rate increases with the streamwise wavenumber (Connaughton *et al.* 2010). Both of these results are in agreement with the findings in this work. However, there is a significant difference with the SSST framework. In modulational instability, the jet formation mechanism requires two main components: the first component is a finite-amplitude cross-stream Rossby wave that is taken *a priori* as the initial perturbation and is assumed to be excited by perturbation instability (for example, baroclinic instability) of the large-scale flow. The second component is the non-linear eddy–eddy interactions that actively participate in the jet forming process through three or four-wave interactions. As a result only a single wave is assumed to support the mean flow with the nonlinear interactions acting as a catalyst for the energy transfer. In contrast, SSST does not require the existence of such finite-amplitude waves and the mean flow is supported by its interaction with a very broad spectrum of waves rather than with a single wave. In addition, the eddy–eddy interactions do not participate in the energy transfer process. Nevertheless, it is worth noting that a special case of the structural instability that would resemble the modulational instability settings (although this would not be a one-to-one correspondence), would be to take the limit of a spatially correlated forcing ($\delta \to \infty$). In this limit, the mean flow is supported by a single cross-stream wave that is stochastically excited without however the catalytic

https://doi.org/10.1017/jfm.2011.228 Published online by Cambridge University Press

action of the eddy–eddy interactions. The main results in this work were found to be insensitive to such a choice, as the growth rate does not depend qualitatively on the choice of δ (cf. figure 4*c*).

8. Conclusions

Large-scale mean jets that are maintained by the very eddies they support, are commonly observed in turbulent fluids. Stability analysis of the coupled eddy-mean flow system is examined in this work within the framework of SSST. In the context of SSST, the average eddy field and the average flow form a coupled dynamical system. The distribution of the eddy momentum fluxes associated with the structure of the large-scale flow is obtained using a linear STM and the resulting Reynolds stress divergence forces the mean momentum equation.

Using SSST, the structural stability of a flow with no mean velocity, subjected to a homogeneous stochastic excitation is examined. The eigenvalues of the linear operator governing the evolution of mean flow perturbations and the associated eddy statistics were calculated for the zero mean flow equilibrium state. The structural stability was found to depend on the sensitivity of the Reynolds stress divergence to changes in the mean flow as quantified by the eigenvalues of the corresponding operator in the quasi-static limit. Calculation of the eigenvalues of this sensitivity operator, revealed two opposing physical mechanisms underlying the structural instability. The first is advection of the eddy vorticity by the infinitesimal jet perturbation, producing a Reynolds stress divergence that is destabilizing. In the physically relevant regime in which the mean flow perturbations have a large scale compared to the eddy scale, eddy vorticity advection was found to act exactly as a diffusion operator with a negative diffusion coefficient. Therefore, the driving mechanism for the emergence of jets is shearing of the eddies by the mean flow. Opposing this tendency, is advection of the vorticity gradient of the mean flow perturbation by the eddies, producing a Reynolds stress divergence that is stabilizing. Advection of the mean flow vorticity gradient was found to act as a hyper-diffusion or as a diffusion operator (depending on the streamwise scale of the eddy field) for mean flow perturbations of large width. When the forcing excites eddies with larger streamwise than cross-stream scales, the diffusion coefficient resulting from each of these two processes was found to be the same and to depend only on the ratio of the eddy excitation over the eddy dissipation. Similar results were obtained when we considered forcing in cross-stream velocity, or in generalized energy coordinates and when we used a second-order diffusion instead of linear damping as eddy dissipation. As a result, the characteristics of the physical mechanisms underlying jet emergence are qualitatively independent of the details of the forcing and of the eddy dissipation.

Structural instability and jet formation were found to occur if two necessary conditions were met. The first condition is that the Reynolds stress divergence tends to reinforce the mean flow perturbation, i.e. if the Reynolds stress divergence produced by eddy vorticity advection dominates. This condition is met if the eddies have scales smaller that a certain minimum scale. Since this minimum scale was found to be a decreasing function of the forcing correlation scale, a finite forcing correlation is needed for destabilizing Reynolds stresses. The second condition is that the eddy excitation should be above a certain threshold, so that the Reynolds stress divergence can overcome the mean flow dissipation. Although the coupled system was found to be unstable for a range of streamwise and mean flow wavenumbers, the maximum growth rate occurs for a jet structure having a width proportional to the streamwise

https://doi.org/10.1017/jfm.2011.228 Published online by Cambridge University Press

wavelength of the most energetic eddies. For linear eddy dissipation, the maximum growth rate was found to be proportional to the streamwise wavenumber of the eddies, whereas for diffusive eddy dissipation, the maximum growth rate is bounded due to the attenuation of smaller width jets.

This research was supported by the Hellenic Scholarship Foundation under an IKY grant and by the EU FP-7 under the PIRG03-GA-2008-230958 Marie Curie Grant. The authors would like to thank three anonymous reviewers for their useful comments that helped improve the manuscript.

Appendix A. Calculation of the structural stability and the Reynolds stress sensitivity operator in the absence of diffusion

The equations for the evolution of small perturbations $\delta \boldsymbol{U}$, $\delta \boldsymbol{C}$ around the equilibrium values of mean velocity $\boldsymbol{U}^E$ and enstrophy covariance $\boldsymbol{C}^E$ are

$$\frac{\mathrm{d}\delta \boldsymbol{C}}{\mathrm{d}t} = \boldsymbol{A}^E \delta \boldsymbol{C} + \delta \boldsymbol{C} \boldsymbol{A}^{E\dagger} + \left(\frac{\partial \boldsymbol{A}^E}{\partial \boldsymbol{U}} \delta \boldsymbol{U}\right) \boldsymbol{C}^E + \boldsymbol{C}^E \left(\frac{\partial \boldsymbol{A}^E}{\partial \boldsymbol{U}} \delta \boldsymbol{U}\right)^{\dagger}, \tag{A 1}$$

$$\frac{\mathrm{d}\delta \boldsymbol{U}}{\mathrm{d}t} = \frac{\partial \boldsymbol{R}}{\partial \boldsymbol{C}} \delta \boldsymbol{C} - r \delta \boldsymbol{U}. \tag{A 2}$$

For the equilibrium with no mean flow, $\boldsymbol{U}^E = 0$, the corresponding enstrophy covariance is given by (3.1) and

$$\boldsymbol{A}^E = -r\boldsymbol{I}. \tag{A 3}$$

Changes in the mean flow alter both the advection of eddy vorticity and the mean vorticity gradient that is advected by the eddies, resulting in a total change of the dynamics that is given by

$$\frac{\partial \boldsymbol{A}^E}{\partial \boldsymbol{U}} \delta \boldsymbol{U} = -\mathrm{i}k\,\mathrm{diag}(\delta \boldsymbol{U}) + \mathrm{i}k\,\mathrm{diag}(\boldsymbol{D}^2 \delta \boldsymbol{U}) \Delta^{-1}. \tag{A 4}$$

By substituting (3.1), (A 3) and (A 4) into (A 1)–(A 2), and considering separate equations for the real, $\delta \boldsymbol{C}^R$, and imaginary, $\delta \boldsymbol{C}^I$, parts of the enstrophy covariance perturbation, we obtain

$$\frac{\mathrm{d}\delta \boldsymbol{C}^R}{\mathrm{d}t} = -2r \delta \boldsymbol{C}^R, \tag{A 5}$$

$$\begin{aligned}\frac{\mathrm{d}\delta \boldsymbol{C}^I}{\mathrm{d}t} = -2r \delta \boldsymbol{C}^I &- \frac{k\epsilon}{2r} [\mathrm{diag}(\delta \boldsymbol{U}) \boldsymbol{Q} - \boldsymbol{Q}\,\mathrm{diag}(\delta \boldsymbol{U})] \\ &+ \frac{k\epsilon}{2r} \{\mathrm{diag}(\boldsymbol{D}^2 \delta \boldsymbol{U}) \Delta^{-1} \boldsymbol{Q} - \boldsymbol{Q} [\mathrm{diag}(\boldsymbol{D}^2 \delta \boldsymbol{U}) \Delta^{-1}]^{\dagger}\},\end{aligned} \tag{A 6}$$

$$\frac{\mathrm{d}\delta \boldsymbol{U}}{\mathrm{d}t} = -\frac{k}{2} \mathrm{vecd}(\Delta^{-1} \delta \boldsymbol{C}^I) - r \delta \boldsymbol{U}. \tag{A 7}$$

We first apply the vec operator to (A 6) and use the identity (B 8), as well as the fact that Δ^{-1} is Hermitian to obtain

$$\frac{\mathrm{d}}{\mathrm{d}t} \mathrm{vec}(\delta \boldsymbol{C}^I) = -2r\ \mathrm{vec}(\delta \boldsymbol{C}^I) + \boldsymbol{L}^{IU} \delta \boldsymbol{U}, \tag{A 8}$$

where

$$\boldsymbol{L}^{IU} = -\frac{\epsilon k}{2r} \{\boldsymbol{Q} * \boldsymbol{I} - \boldsymbol{I} * \boldsymbol{Q} - [(\boldsymbol{Q}\Delta^{-1}) * \boldsymbol{I} - \boldsymbol{I} * (\boldsymbol{Q}\Delta^{-1})] \boldsymbol{D}^2\}. \tag{A 9}$$

https://doi.org/10.1017/jfm.2011.228 Published online by Cambridge University Press

We then use the identity $\mathrm{vecd}(\Delta^{-1}\delta\boldsymbol{C}^I)=\boldsymbol{J}\mathrm{vec}(\Delta^{-1}\delta\boldsymbol{C}^I)$ proven in (B 11) as well as (B 3), to rewrite (A 7) as

$$\frac{\mathrm{d}}{\mathrm{d}t}\delta\boldsymbol{U}=\boldsymbol{L}^{UI}\mathrm{vec}(\delta\boldsymbol{C}^I)-r\delta\boldsymbol{U}, \tag{A 10}$$

where

$$\boldsymbol{L}^{UI}=-\frac{k}{2}\boldsymbol{J}(\boldsymbol{I}\otimes\Delta^{-1}). \tag{A 11}$$

As shown above, the $N\times N^2$ matrix $\boldsymbol{J}$ extracts the diagonal elements of a matrix that has been turned into a vector through the vec operator (cf. (B 11)). It is the matrix with non-zeros elements $J_{i,(i-1)(N+1)}=1$, that also satisfies $\boldsymbol{J}\boldsymbol{J}^T=\boldsymbol{I}$. By construction, it has N linearly independent columns and as a result $\mathrm{rank}(\boldsymbol{J})=N$. The $N\times N^2$ matrix $\boldsymbol{L}^{UI}$ given by (3.3) is also of rank N and has a null space of dimension N^2-N. If we rewrite (A 5), (A 8) and (A 10) in the notation of (2.17), we obtain the expression of the structural stability operator given by (3.2).

The sensitivity operator $\boldsymbol{S}=\boldsymbol{L}^{UI}\boldsymbol{L}^{IU}$ can be written in the form

$$\boldsymbol{S}=\frac{\epsilon k^2}{4r^2}\boldsymbol{J}(\boldsymbol{I}\otimes\Delta^{-1})\{\boldsymbol{Q}*\boldsymbol{I}-\boldsymbol{I}*\boldsymbol{Q}-[(\boldsymbol{Q}\Delta^{-1})*\boldsymbol{I}-\boldsymbol{I}*(\boldsymbol{Q}\Delta^{-1})]\boldsymbol{D}^2\}, \tag{A 12}$$

or, alternatively, using (B 9)

$$\boldsymbol{S}=\frac{\epsilon k^2}{4r^2}\boldsymbol{J}\{\boldsymbol{Q}*\Delta^{-1}-\boldsymbol{I}*(\Delta^{-1}\boldsymbol{Q})-[(\boldsymbol{Q}\Delta^{-1})*\Delta^{-1}-\boldsymbol{I}*(\Delta^{-1}\boldsymbol{Q}\Delta^{-1})]\boldsymbol{D}^2\}. \tag{A 13}$$

Finally, applying (B 6), we obtain

$$\boldsymbol{S}=\frac{\epsilon k^2}{4r}\{[\boldsymbol{Q}\circ\Delta^{-1}-\boldsymbol{I}\circ(\Delta^{-1}\boldsymbol{Q})]-[\Delta^{-1}\circ(\boldsymbol{Q}\Delta^{-1})-\boldsymbol{I}\circ(\Delta^{-1}\boldsymbol{Q}\Delta^{-1})]\boldsymbol{D}^2\}, \tag{A 14}$$

which is (4.1).

Appendix B. Identities involving the vec, vecd operators and the Khatri–Rao, Hadamard and Kronecker products

The Kronecker product of the $k\times l$ matrix $\boldsymbol{A}$ with the $m\times n$ matrix $\boldsymbol{B}$ is the $km\times ln$ matrix $\boldsymbol{A}\otimes\boldsymbol{B}$ defined as

$$\boldsymbol{A}\otimes\boldsymbol{B}=\begin{pmatrix} A_{11}\boldsymbol{B} & \dots & A_{1l}\boldsymbol{B} \\ \cdot & \cdots & \cdot \\ \cdot & \cdots & \cdot \\ A_{k1}\boldsymbol{B} & \dots & A_{kl}\boldsymbol{B}\end{pmatrix}. \tag{B 1}$$

The Khatri–Rao product of two matrices $\boldsymbol{A}$ and $\boldsymbol{B}$ with columns $\boldsymbol{a}_i$ and $\boldsymbol{b}_i$, respectively, is defined as

$$\boldsymbol{A}*\boldsymbol{B}=[\boldsymbol{a}_1\otimes\boldsymbol{b}_1\ \boldsymbol{a}_2\otimes\boldsymbol{b}_2\ \dots\ \boldsymbol{a}_n\otimes\boldsymbol{b}_n]. \tag{B 2}$$

Throughout the text, the following identities concerning the vec, vecd operators and the Khatri–Rao, Hadamard and Kronecker products are used (Brewer 1978; Graham 1981):

$$\mathrm{vec}(\boldsymbol{A}\boldsymbol{X}\boldsymbol{B})=(\boldsymbol{B}^{\mathrm{T}}\otimes\boldsymbol{A})\mathrm{vec}(\boldsymbol{X}), \tag{B 3}$$

$$\mathrm{vec}(\boldsymbol{I}\circ\boldsymbol{A})=\mathrm{diag}\,(\mathrm{vec}(\boldsymbol{I}))\,\mathrm{vec}(\boldsymbol{A}), \tag{B 4}$$

https://doi.org/10.1017/jfm.2011.228 Published online by Cambridge University Press

$$\mathrm{vecd}(\boldsymbol{A}) = (\boldsymbol{I} \circ \boldsymbol{A})\,\boldsymbol{e}, \tag{B 5}$$

$$\boldsymbol{J}(\boldsymbol{A} * \boldsymbol{B}) = \boldsymbol{A} \circ \boldsymbol{B}, \tag{B 6}$$

$$(\boldsymbol{e} \otimes \boldsymbol{I})\mathrm{diag}\,(\mathrm{vec}(\boldsymbol{I})) = \boldsymbol{J}, \tag{B 7}$$

$$\mathrm{vec}(\boldsymbol{AYB}) = \left(\boldsymbol{B}^{\mathrm{T}} * \boldsymbol{A}\right)\mathrm{vecd}(\boldsymbol{Y}), \tag{B 8}$$

$$(\boldsymbol{A} \otimes \boldsymbol{B})(\boldsymbol{C} * \boldsymbol{D}) = (\boldsymbol{AC}) * (\boldsymbol{BD}), \tag{B 9}$$

where $\boldsymbol{A}$, $\boldsymbol{B}$, $\boldsymbol{C}$, $\boldsymbol{D}$, $\boldsymbol{X}$ are matrices. $\boldsymbol{Y}$ is a diagonal matrix, $\boldsymbol{I}$ is the identity matrix, $\boldsymbol{e}^{\mathrm{T}} = [1\ 1\ \ldots\ 1]$ and $\boldsymbol{J}$ is the $N \times N^2$ selection matrix given in Appendix A. T denotes the transpose of a matrix, $\circ$ denotes the Hadamard–Schur entrywise product and $*$ denotes the Khatri–Rao product. Using (B 3)–(B 8), it can be readily shown that the following identities hold as well:

$$\mathrm{vec}\,([\mathrm{diag}(\boldsymbol{a}), \boldsymbol{B}]) = \left(\boldsymbol{B}^{T} * \boldsymbol{I} - \boldsymbol{I} * \boldsymbol{B}\right)\boldsymbol{a}, \tag{B 10}$$

$$\begin{aligned}\mathrm{vecd}(\boldsymbol{A}) = \mathrm{vec}\,[\mathrm{vecd}(\boldsymbol{A})] = \mathrm{vec}\,[(\boldsymbol{I} \circ \boldsymbol{A})\,\boldsymbol{e}] = (\boldsymbol{e} \otimes \boldsymbol{I})\mathrm{vec}\,(\boldsymbol{I} \circ \boldsymbol{A}) \\ = (\boldsymbol{e} \otimes \boldsymbol{I})\mathrm{diag}\,(\mathrm{vec}(\boldsymbol{I}))\,\mathrm{vec}(\boldsymbol{A}) = \boldsymbol{J}\mathrm{vec}(\boldsymbol{A}),\end{aligned} \tag{B 11}$$

where $\boldsymbol{a}$ is a vector.

Appendix C. Analytic calculation of the eigenvalues of the flux sensitivity operator

An $N \times N$ matrix $\boldsymbol{C}$ is circulant when its entries satisfy $C_{i,j} = C_{1,j-i \bmod N}$. That is, each row is a cyclic shift of the row above it. An elaborate discussion of circulant matrices can be found in Davis (1978). Consider now the $N \times N$ circulant matrix $\boldsymbol{H}$, where N is taken without loss of generality to be an odd number. The first line of $\boldsymbol{H}$ can be written as

$$\boldsymbol{h} = [h_0\ h_1\ \cdots\ h_{(N-1)/2}\ h_{-(N-1)/2}\ h_{-(N-1)/2+1} \cdots\ h_{-2}\ h_{-1}], \tag{C 1}$$

and for real symmetric $\boldsymbol{H}$ satisfies $h_{-n} = h_n$. The mth eigenvalue ($1 \leqslant m \leqslant N$) is the discrete Fourier transform (DFT) of the elements of the matrix

$$\lambda_m^{\boldsymbol{H}} = \sum_{n=-(N-1)/2}^{(N-1)/2} h_n\,\mathrm{e}^{-2\mathrm{i}\pi nm/N}. \tag{C 2}$$

It is real and satisfies the relation

$$\lambda_{-m}^{\boldsymbol{H}} = \sum_{n=-(N-1)/2}^{(N-1)/2} h_n\,\mathrm{e}^{2\mathrm{i}\pi nm/N} = \left(\sum_{n=-(N-1)/2}^{(N-1)/2} h_n\,\mathrm{e}^{-2\mathrm{i}\pi nm/N}\right)^{*} = \left(\lambda_m^{\boldsymbol{H}}\right)^{*} = \lambda_m^{\boldsymbol{H}}. \tag{C 3}$$

Therefore, there are $(N-1)/2$ double eigenvalues and one single. In addition, if the eigenvalues of a circulant matrix are known, then the elements of the matrix are the inverse DFT of the eigenvalues

$$h_m = \frac{1}{N}\sum_{n=-(N-1)/2}^{(N-1)/2} \lambda_n^{\boldsymbol{H}}\,\mathrm{e}^{2\mathrm{i}\pi nm/N}. \tag{C 4}$$

https://doi.org/10.1017/jfm.2011.228 Published online by Cambridge University Press

The eigenvalues of the Hadamard product of two circulant matrices is given by the convolution of the eigenvalues of the two matrices:

$$\lambda_n^{\boldsymbol{H}\circ\boldsymbol{G}} = \sum_{m=-\frac{N-1}{2}}^{\frac{N-1}{2}} h_m g_m \,\mathrm{e}^{-2\mathrm{i}\pi nm/N} = \frac{1}{N^2}\sum_{m=-\frac{N-1}{2}}^{\frac{N-1}{2}}\sum_{k=-\frac{N-1}{2}}^{\frac{N-1}{2}}\sum_{l=-\frac{N-1}{2}}^{\frac{N-1}{2}} \lambda_k^{\boldsymbol{H}}\,\mathrm{e}^{2\mathrm{i}\pi mk/N}\lambda_l^{\boldsymbol{G}}\,\mathrm{e}^{2\mathrm{i}\pi ml/N}\,\mathrm{e}^{-2\mathrm{i}\pi nm/N}$$

$$= \frac{1}{N}\sum_{k=-\frac{N-1}{2}}^{\frac{N-1}{2}}\sum_{l=-\frac{N-1}{2}}^{\frac{N-1}{2}} \lambda_k^{\boldsymbol{H}}\lambda_l^{\boldsymbol{G}}\delta_{(k+l-n)0 \ mod \ N}$$

$$= \frac{1}{N}\sum_{k=-\frac{N-1}{2}}^{\frac{N-1}{2}} \lambda_k^{\boldsymbol{H}}\lambda_{n-k \ mod \ N}^{\boldsymbol{G}}. \tag{C 5}$$

For $n>0$, (C 5) can be rewritten as

$$\lambda_n^{\boldsymbol{H}\circ\boldsymbol{G}} = \frac{1}{N}\sum_{m=-\frac{N-1}{2}}^{-\frac{N-1}{2}+n-1} \lambda_m^{\boldsymbol{H}}\lambda_{n-m-N}^{\boldsymbol{G}} + \frac{1}{N}\sum_{m=-\frac{N-1}{2}+n}^{\frac{N-1}{2}} \lambda_m^{\boldsymbol{H}}\lambda_{n-m}^{\boldsymbol{G}}, \tag{C 6}$$

and for $n=0$

$$\lambda_0^{\boldsymbol{H}\circ\boldsymbol{G}} = \frac{1}{N}\sum_{n=-\frac{N-1}{2}}^{\frac{N-1}{2}} \lambda_n^{\boldsymbol{H}}\lambda_n^{\boldsymbol{G}}. \tag{C 7}$$

As a result, the eigenvalues s_n^{ad} and s_n^{vg} are given by

$$s_n^{ad} = \lambda_n^{\Delta^{-1}\circ\boldsymbol{Q}} - \lambda_n^{\boldsymbol{I}\circ(\Delta^{-1}\boldsymbol{Q})} = \frac{1}{N}\sum_{m=-\frac{N-1}{2}}^{\frac{N-1}{2}} \lambda_m^{\Delta^{-1}}\left(\lambda_{n-m \ mod \ N}^{\boldsymbol{Q}} - \lambda_m^{\boldsymbol{Q}}\right), \tag{C 8}$$

$$s_n^{vg} = \lambda_n^{[\Delta^{-1}\circ(\boldsymbol{Q}\Delta^{-1})]\boldsymbol{D}^2} - \lambda_n^{[\boldsymbol{I}\circ(\Delta^{-1}\boldsymbol{Q}\Delta^{-1})]\boldsymbol{D}^2} = \frac{\lambda_n^{\boldsymbol{D}^2}}{N}\sum_{m=-\frac{N-1}{2}}^{\frac{N-1}{2}} \lambda_m^{\Delta^{-1}}\left(\lambda_{n-m \ mod \ N}^{\boldsymbol{Q}\Delta^{-1}} - \lambda_m^{\boldsymbol{Q}\Delta^{-1}}\right), \tag{C 9}$$

where

$$\lambda_n^{\Delta^{-1}} = -\frac{1}{k^2+n^2}, \quad \lambda_n^{\boldsymbol{D}^2} = -n^2, \tag{C 10}$$

are the eigenvalues of Δ^{-1} and $\boldsymbol{D}^2$, and $\lambda_n^{\boldsymbol{Q}}$ are the eigenvalues of $\boldsymbol{Q}$ to be calculated.

The eigenvalues of $\boldsymbol{Q}$ are given by $\lambda_n^{\boldsymbol{Q}} = (\lambda_n^{\boldsymbol{F}})^2$, where $\lambda_m^{\boldsymbol{F}}$ are the eigenvalues of the forcing matrix $\boldsymbol{F}$. The first line of $\boldsymbol{F}$ is:

$$f_m = A\left(\mathrm{e}^{-(m\delta y)^2/\delta^2} + \mathrm{e}^{-(2\pi - m\delta y)^2/\delta^2} + \mathrm{e}^{-(2\pi + m\delta y)^2/\delta^2}\right), \tag{C 11}$$

where A is the forcing amplitude, δ is the forcing correlation scale and δy is the discretization scale. The eigenvalues of $\boldsymbol{F}$ are then given according to (C 2) by

$$\lambda_n^{\boldsymbol{F}} = \frac{A}{\delta y}\sum_{m=-(N-1)/2}^{(N-1)/2}\left(\mathrm{e}^{-y_m^2/\delta^2} + \mathrm{e}^{-(2\pi - y_m)^2/\delta^2} + \mathrm{e}^{-(2\pi + y_m)^2/\delta^2}\right)\mathrm{e}^{-\mathrm{i}ny_m}\delta y, \tag{C 12}$$

where $y_m = m\delta y = 2m\pi/N$. The major contribution to the sum comes from the terms near $m=0$ for which $|f_0 - f_1|/|f_0| \ O(\delta y^2)$. Therefore, in the continuous limit ($\delta y \to 0$), the sum can be approximated by the integral:

https://doi.org/10.1017/jfm.2011.228 Published online by Cambridge University Press

$$\lambda_n^{\boldsymbol{F}} = \frac{A}{\delta y}\int_{-\pi}^{\pi}\left(\mathrm{e}^{-y^2/d^2} + \mathrm{e}^{-(2\pi-y)^2/\delta^2} + \mathrm{e}^{-(2\pi+y)^2/\delta^2}\right)\mathrm{e}^{-\mathrm{i}ny}\,\mathrm{d}y$$
$$= \frac{A\delta\sqrt{\pi}}{2\delta y}\,\mathrm{e}^{-n^2\delta^2/4}\left[\mathrm{erf}\left(\frac{3\pi}{\delta} + \frac{\mathrm{i}\delta n\pi}{2}\right) + \mathrm{erf}\left(\frac{3\pi}{\delta} - \frac{\mathrm{i}\delta n\pi}{2}\right)\right], \quad (C\,13)$$

that in the limit of $\delta \ll 1$ becomes $\lambda_n^{\boldsymbol{F}} = (A\delta\sqrt{\pi}/\delta y)\,\mathrm{e}^{-n^2\delta^2/4}$, yielding:

$$\lambda_n^{\boldsymbol{Q}} = \frac{A^2\delta^2\pi}{\delta y^2}\,\mathrm{e}^{-n^2\delta^2/2}. \quad (C\,14)$$

The forcing amplitude is constrained to impart an input variance that is equal to the energy of a constant flow of unit velocity

$$\lim_{\delta y\to 0}\mathrm{tr}\,(\boldsymbol{MQ}) = \int_0^{2\pi}\frac{\boldsymbol{U}^2}{2}\mathrm{d}y = \pi, \quad (C\,15)$$

where

$$\boldsymbol{M} = -\frac{\delta y}{4}\Delta^{-1}, \quad (C\,16)$$

is the metric such that the eddy energy is given by the inner product $E = \boldsymbol{q}^\dagger\boldsymbol{M}\boldsymbol{q}$. From (C 10) and (C 14), we obtain that the forcing normalization is

$$\frac{1}{A^2} = \frac{\delta^2}{4\delta y}\sum_{m=-(N-1)/2}^{(N-1)/2}\frac{\mathrm{e}^{-m^2\delta^2/2}}{k^2+m^2}. \quad (C\,17)$$

C.1. *Proof that the eigenvalues of* $\boldsymbol{S}^{ad}$ *and* $\boldsymbol{S}^{vg}$ *are non-negative*

We rewrite (C 8) and (C 9) using (C 6)

$$s_n^{ad} = \frac{1}{N}\sum_{m=-\frac{N-1}{2}}^{-\frac{N-1}{2}+n-1}\lambda_m^{\Delta^{-1}}\left(\lambda^{\boldsymbol{Q}}_{n-m-N} - \lambda^{\boldsymbol{Q}}_m\right) + \frac{1}{N}\sum_{m=-\frac{N-1}{2}+n}^{\frac{N-1}{2}}\lambda_m^{\Delta^{-1}}\left(\lambda^{\boldsymbol{Q}}_{n-m} - \lambda^{\boldsymbol{Q}}_m\right), \quad (C\,18)$$

$$s_n^{vg} = -\frac{n^2}{N}\sum_{m=-\frac{N-1}{2}}^{-\frac{N-1}{2}+n-1}\lambda_m^{\Delta^{-1}}\left(\lambda^{\boldsymbol{Q}\Delta^{-1}}_{n-m-N} - \lambda^{\boldsymbol{Q}\Delta^{-1}}_m\right) - \frac{n^2}{N}\sum_{m=-\frac{N-1}{2}+n}^{\frac{N-1}{2}}\lambda_m^{\Delta^{-1}}\left(\lambda^{\boldsymbol{Q}\Delta^{-1}}_{n-m} - \lambda^{\boldsymbol{Q}\Delta^{-1}}_m\right). \quad (C\,19)$$

Assume without loss of generality that n is an even integer. By expanding the sums in (C 18) and (C 19), reorganizing the terms and taking common factors, it can be shown that (C 18) and (C 19) can be rewritten as

$$s_n^{ad} = \frac{1}{N}\sum_{m=0}^{\frac{N-n-1}{2}-1}\left(\lambda^{\Delta^{-1}}_{\frac{N-1}{2}-m-n} - \lambda^{\Delta^{-1}}_{\frac{N-1}{2}-m}\right)\left(\lambda^{\boldsymbol{Q}}_{\frac{N-1}{2}-m} - \lambda^{\boldsymbol{Q}}_{\frac{N-1}{2}-m-n}\right)$$
$$+ \frac{1}{N}\sum_{m=0}^{\frac{n}{2}}\left(\lambda^{\Delta^{-1}}_{\frac{N-1}{2}-n+1+m} - \lambda^{\Delta^{-1}}_{\frac{N-1}{2}-m}\right)\left(\lambda^{\boldsymbol{Q}}_{\frac{N-1}{2}-m} - \lambda^{\boldsymbol{Q}}_{\frac{N-1}{2}-n+1+m}\right), \quad (C\,20)$$

$$s_n^{vg} = -\frac{n^2}{N}\sum_{m=0}^{\frac{N-n-1}{2}-1}\left(\lambda^{\Delta^{-1}}_{\frac{N-1}{2}-m-n} - \lambda^{\Delta^{-1}}_{\frac{N-1}{2}-m}\right)\left(\lambda^{\boldsymbol{Q}\Delta^{-1}}_{\frac{N-1}{2}-m} - \lambda^{\boldsymbol{Q}\Delta^{-1}}_{\frac{N-1}{2}-m-n}\right)$$
$$- \frac{n^2}{N}\sum_{m=0}^{\frac{N-n-1}{2}-1}\left(\lambda^{\Delta^{-1}}_{\frac{N-1}{2}-n+1+m} - \lambda^{\Delta^{-1}}_{\frac{N-1}{2}-m}\right)\left(\lambda^{\boldsymbol{Q}\Delta^{-1}}_{\frac{N-1}{2}-m} - \lambda^{\boldsymbol{Q}\Delta^{-1}}_{\frac{N-1}{2}-n+1+m}\right). \quad (C\,21)$$

https://doi.org/10.1017/jfm.2011.228 Published online by Cambridge University Press

Since $\lambda^{\Delta^{-1}}_{\frac{N-1}{2}-m} > \lambda^{\Delta^{-1}}_{\frac{N-1}{2}-m-n}$ and $\lambda^{\mathbf{Q}}_{\frac{N-1}{2}-m-n} > \lambda^{\mathbf{Q}}_{\frac{N-1}{2}-m}$ it follows from (C 20) and (C 21) that $s_n^{ad} > 0$ and $s_n^{vg} > 0$.

C.2. *Eigenvalues for jet structures with small mean flow wavenumber*

Analytic calculation of the eigenvalues s_n^{ad}, s_n^{vg} for low n proceeds as follows. First of all, note that the constant mean flow eigenstructure is neutral as it can be readily shown that for $n=0$, (C 8) and (C 9) yield: $s_0^{ad} = s_0^{vg} = 0$. Using (C 6) and for eigenstructures with small mean flow wavenumber satisfying $l_c \gg n\delta y$ (that also satisfy $(N-1)/2 - n \gg 1$), (C 8) and (C 9) can be approximated by

$$s_n^{ad} \simeq \frac{1}{N}\sum_{m=-\frac{N-1}{2}}^{\frac{N-1}{2}} \lambda_m^{\Delta^{-1}}\lambda^{\mathbf{Q}}_{n-m} - \frac{1}{N}\sum_{m=-\frac{N-1}{2}}^{\frac{N-1}{2}} \lambda_m^{\Delta^{-1}}\lambda_m^{\mathbf{Q}} = \frac{1}{N}\sum_{m=-\frac{N-1}{2}}^{\frac{N-1}{2}} (p_1(m,n) - p_1(m,0)), \quad \text{(C 22)}$$

and

$$s_n^{vg} \simeq \frac{\lambda_n^{\mathbf{D}^2}}{N}\sum_{m=-\frac{N-1}{2}}^{\frac{N-1}{2}} \lambda_m^{\Delta^{-1}}\left(\lambda^{\mathbf{Q}\Delta^{-1}}_{n-m} - \lambda_m^{\Delta^{-1}}\lambda_m^{\mathbf{Q}}\right) = \frac{n^2}{N}\sum_{m=-\frac{N-1}{2}}^{\frac{N-1}{2}} (p_2(m,n) - p_2(m,0)), \quad \text{(C 23)}$$

where

$$p_1(m,n) = \lambda_m^{\Delta^{-1}}\lambda^{\mathbf{Q}}_{n-m} = -\frac{A^2\delta^2\pi}{\delta y^2}\frac{\mathrm{e}^{-(n-m)^2\delta^2/2}}{k^2+m^2}, \quad \text{(C 24)}$$

and $p_2(m,n) = -\lambda_m^{\Delta^{-1}}\lambda^{\mathbf{Q}\Delta^{-1}}_{n-m} = p_1(n,m)/[k^2 + (m-n)^2]$. For $n \ll 2\pi$, the major contribution to the sums comes from the terms close to $m=0$ for which

$$S = \left|\frac{p_i(0,n) - p_i(1,n)}{p_i(0,n)}\right| \simeq \frac{1}{(k^2+1)^i}. \quad \text{(C 25)}$$

In the limit of large streamwise wavenumber ($kl_c \gg 1$), $S \ll 1$ and the sums in (C 22) and (C 23) can be approximated by integrals that in the continuous limit and after changing variables become

$$s_n^{ad} \simeq -\frac{A^2\delta^2\pi}{N\delta y^2}\int_{-\infty}^{\infty}\frac{\mathrm{e}^{-(n-t)^2\delta^2/2} - \mathrm{e}^{-t^2\delta^2/2}}{k^2+t^2}\,\mathrm{d}t, \quad \text{(C 26)}$$

$$s_n^{vg} \simeq -\frac{A^2\delta^2\pi}{N\delta y^2}n^2\int_{-\infty}^{\infty}\left(\frac{\mathrm{e}^{-(n-t)^2\delta^2/2}}{(k^2+t^2)(k^2+(n-t)^2)} - \frac{\mathrm{e}^{-t^2\delta^2/2}}{(k^2+t^2)^2}\right)\mathrm{d}t. \quad \text{(C 27)}$$

Similarly, (C 17) is reduced to

$$\frac{1}{A^2} = \frac{\delta^2}{4\delta y}\int_{-\infty}^{\infty}\frac{\mathrm{e}^{-t^2\delta^2/2}}{k^2+t^2}\,\mathrm{d}t = 1, \quad \text{(C 28)}$$

yielding:

$$A = \sqrt{\frac{4k\delta y\exp(-k^2\delta^2/2)}{\delta^2\pi\mathrm{erfc}\left(k\delta/\sqrt{2}\right)}}. \quad \text{(C 29)}$$

https://doi.org/10.1017/jfm.2011.228 Published online by Cambridge University Press

Expanding the integrands in powers of n, we obtain after substitution of A from (C 29) that s_n^{ad} and s_n^{vg} are given by (4.5), where

$$c_2(k,\delta) = \delta^2\left(1 + k^2\delta^2 - \frac{\sqrt{2\pi}\delta k\, \mathrm{e}^{-k^2\delta^2/2}}{\pi \mathrm{erfc}(k\delta/\sqrt{2})}\right), \tag{C 30}$$

$$c_3(k\delta) = \frac{1}{12}\left(3 - 3k^4\delta^4 - 2k^6\delta^6 + \sqrt{2\pi}k\delta(3 + k^2\delta^2 + 2k^4\delta^4)\frac{\mathrm{e}^{-k^2\delta^2/2}}{\pi \mathrm{erfc}(k\delta/\sqrt{2})}\right). \tag{C 31}$$

For $k\delta \gg 1$, (C 30) and (C 31) can be further approximated to yield

$$c_2 = 2/k^2, \quad c_3 = 2 \tag{C 32}$$

and for $k\delta \ll 1$. they become

$$c_2 = \delta^2(1 - \sqrt{2/\pi}k\delta), \quad c_3 = (1/4)(1 + \sqrt{2/\pi}k\delta). \tag{C 33}$$

As a result, in the limit of correlated forcing ($\delta \to \infty$), $s_n \simeq (\epsilon k^2/4r)(2n^2/k^2 - 2n^4/k^4)$ is positive for the gravest mode ($n = 1$) only if $k > k_c = 1$. For $k\delta \ll 1$, $s_n \simeq (\epsilon k^2/4r)(\delta^2 n^2 - n^4/4k^4)$ and the corresponding cut-off wavenumber is $k_c = 1/\sqrt{2\delta}$.

In the limit of low streamwise wavenumber ($kl_c \ll 1$), the sums in (C 17), (C 22) and (C 23) are dominated by the $m = 0$ terms. Keeping only this term and in the limit of $n\delta y \ll l_c$, (C 17), (C 22) and (C 23) become

$$A = \sqrt{\frac{4k^2\delta y}{\delta^2}}, \tag{C 34}$$

$$s_n^{ad} \simeq -\frac{A^2\delta^2\pi}{N\delta y^2}\left(\frac{\mathrm{e}^{-n^2\delta^2/2}}{k^2} - \frac{1}{k^2}\right) \simeq \frac{A^2\delta^4\pi}{2N\delta y^2 k^2}n^2 \simeq \delta^2 n^2, \tag{C 35}$$

and

$$s_n^{vg} \simeq -\frac{A^2\delta^2\pi}{N\delta y^2}n^2\left(\frac{\mathrm{e}^{-n^2\delta^2/2}}{k^2(k^2+n^2)} - \frac{1}{k^4}\right) \simeq \frac{A^2\delta^2\pi}{N\delta y^2 k^4}n^2 \simeq \frac{2}{k^2}n^2, \tag{C 36}$$

respectively.

C.3. *Eigenvalues for jet structures with large mean flow wavenumber*

We now calculate an analytic expression for the eigenvalues s_n^{ad}, s_n^{vg} for eigenstructures with large mean flow wavenumber $n\delta y$ $O(l_c/2)$, for which (C 8) and (C 9) can be approximated by

$$s_n^{ad} \simeq \frac{2}{N}\sum_{m=-(N-1)/2+n}^{\frac{N-1}{2}} \lambda_m^{\mathbf{Q}}\lambda_{n-m}^{\Delta^{-1}} - \frac{1}{N}\sum_{m=-\frac{N-1}{2}}^{\frac{N-1}{2}} \lambda_m^{\Delta^{-1}}\lambda_m^{\mathbf{Q}}, \tag{C 37}$$

and

$$s_n^{vg} \simeq \frac{2\lambda_n^{\mathbf{D}^2}}{N}\sum_{m=-(N-1)/2+n}^{\frac{N-1}{2}} \lambda_m^{\mathbf{Q}\Delta^{-1}}\lambda_{n-m}^{\Delta^{-1}} - \frac{\lambda_n^{\mathbf{D}^2}}{N}\sum_{m=-\frac{N-1}{2}}^{\frac{N-1}{2}} \left(\lambda_m^{\Delta^{-1}}\right)^2\lambda_m^{\mathbf{Q}}. \tag{C 38}$$

The second term in (C 37) is equal to -2 due to (C 17). It can also be readily shown that in the limit of large streamwise wavenumbers ($kl_c \gg 1$), the rest of the sums in (C 37) and (C 38) can be approximated by integrals that in the continuous limit and

https://doi.org/10.1017/jfm.2011.228 Published online by Cambridge University Press

for $n\delta y \; O(l_c/2)$ become

$$s_n^{ad} \simeq 2 - \frac{2A^2\delta^2\pi}{N\delta y^2}\int_0^\infty \frac{\mathrm{e}^{-m^2\delta^2/2}}{k^2+(n-m)^2}\,\mathrm{d}m \simeq 2 - \frac{8A^2\delta^2\pi}{N^3\delta y^2}\int_0^\infty \mathrm{e}^{-m^2\delta^2/2}\,\mathrm{d}m, \tag{C 39}$$

$$\begin{aligned} s_n^{vg} &\simeq \frac{2A^2\delta^2\pi}{N\delta y^2}n^2\int_0^\infty \frac{\mathrm{e}^{-m^2\delta^2/2}}{k^2+m^2}\left(\frac{1}{k^2+m^2} - \frac{1}{k^2+(n-m)^2}\right)\mathrm{d}m \\ &\simeq \frac{2A^2\delta^2\pi}{N\delta y^2}n^2\int_0^\infty \frac{\mathrm{e}^{-m^2\delta^2/2}}{k^2+m^2}\left(\frac{1}{k^2+m^2} - \frac{4}{N^2}\right)\mathrm{d}m. \end{aligned} \tag{C 40}$$

After calculation of the integrals and substitution of A by (C 29), (C 39) and (C 40) yield

$$s_n^{ad} \simeq 2 - O(\delta y)^2, \tag{C 41}$$

$$s_n^{vg} \simeq \frac{n^2}{k^2}\left(1 - k^2\delta^2 + \frac{k\delta\sqrt{2\pi}\,\mathrm{e}^{-k^2\delta^2/2}}{\pi\mathrm{erfc}(k\delta/\sqrt{2})}\right) + O(\delta y^2). \tag{C 42}$$

On the other hand, in the limit of low streamwise wavenumbers ($kl_c \ll 1$), the sums in (C 17), (C 37) and (C 38) are dominated by the $n=0$ terms. Keeping only this term, we obtain

$$s_n^{ad} \simeq 2 - O(\delta y)^2, \tag{C 43}$$

$$s_n^{vg} \simeq \frac{A^2\delta^2\pi}{N\delta y^2}\frac{1}{k^4} = \frac{2}{k^2}n^2. \tag{C 44}$$

Therefore, s^{vg} is given by (4.4) with

$$c_1(k\delta) = \begin{cases} 2, & \text{for } kl_c \ll 1, \\ 1 - k^2\delta^2 + k\delta\sqrt{2\pi}\,\mathrm{e}^{-k^2\delta^2/2}/\pi\mathrm{erfc}(k\delta/\sqrt{2}), & \text{for } kl_c \gg 1. \end{cases} \tag{C 45}$$

Appendix D. Calculation of the eigenvalues of the structural stability operator in the presence of diffusion

When the effective eddy dissipation is only diffusive (i.e. $r=0$ and $\nu \neq 0$), it can be readily shown that for $\boldsymbol{U}^E = 0$

$$\boldsymbol{A}^E = \nu\Delta, \tag{D 1}$$

and the corresponding covariance at equilibrium is

$$\boldsymbol{C}^E = -\frac{\epsilon\Delta^{-1}\boldsymbol{Q}}{2\nu}. \tag{D 2}$$

Substituting (D 1), (D 2) and (A 4) into (A 1) and (A 2) and applying the vec operator, we obtain

$$\boldsymbol{L} = \begin{pmatrix} \nu\Delta\oplus\Delta & 0 & 0 \\ 0 & \nu\Delta\oplus\Delta & \boldsymbol{L}^{IUd}/\nu \\ 0 & \boldsymbol{L}^{UI} & \nu\boldsymbol{D}^2 \end{pmatrix}, \tag{D 3}$$

where $\oplus$ denotes the Kronecker sum (the Kronecker sum is defined as $\boldsymbol{A}\oplus\boldsymbol{B} = \boldsymbol{A}\otimes\boldsymbol{I} + \boldsymbol{I}\otimes\boldsymbol{B}$, where $\boldsymbol{I}$ the identity) and

$$\boldsymbol{L}^{IUd} = \frac{k\epsilon}{2}\{(\Delta^{-1}\boldsymbol{Q})*\boldsymbol{I} - \boldsymbol{I}*(\Delta^{-1}\boldsymbol{Q}) - [(\Delta^{-1}\boldsymbol{Q}\Delta^{-1})*\boldsymbol{I} - \boldsymbol{I}*(\Delta^{-1}\boldsymbol{Q}\Delta^{-1})]\boldsymbol{D}^2\}. \tag{D 4}$$

https://doi.org/10.1017/jfm.2011.228 Published online by Cambridge University Press

Similarly to the case of linear eddy dissipation, it can be shown from (D 3) that the stability operator $\boldsymbol{L}$ has $2N^2 - N$ eigenvalues $-\nu[2k^2 + n^2 + m^2]$, $n = 1, \ldots, N$, $m = 1, \ldots, N$ with corresponding eigenvectors having $\delta \boldsymbol{U} = 0$ that are therefore not of interest for the emergence of mean flows. The remaining $2N$ eigenvalues are given by the solution to

$$\det \left\{ \lambda \boldsymbol{I} + \frac{1}{\nu} \boldsymbol{L}^{UI} \left[\lambda \boldsymbol{I}_{N^2} - \nu \Delta \oplus \Delta \right]^{-1} \boldsymbol{L}^{IUd} - \nu \boldsymbol{D}^2 \right\} = 0. \tag{D 5}$$

Assuming that $\nu \ll \lambda$, we can approximate $[\lambda \boldsymbol{I}_{N^2} - \nu \Delta \oplus \Delta]^{-1} \simeq \lambda^{-1} \boldsymbol{I} + \nu \Delta \oplus \Delta / \lambda^2$. Then, (D 5) can be solved perturbatively by expanding the eigenvalues in powers of ν: $\lambda = \nu^{-1/2} \lambda^0 + \nu \lambda^1 + \ldots$ and solving order by order to obtain up to $O(\nu)$

$$\lambda_n^0 = \pm \sqrt{s_n^v}, \quad n = 1, \ldots, N, \tag{D 6}$$

$$\lambda_n^1 = \frac{\lambda_n^{UI\Delta}}{2 s_n^v} - \frac{n^2}{2}, \quad n = 1, \ldots, N. \tag{D 7}$$

Here, s_n^v are the eigenvalues of the $N \times N$ matrix $\boldsymbol{S}^v = \boldsymbol{L}^{UI} \boldsymbol{L}^{IUd}$ and $\lambda_n^{UI\Delta}$ are the eigenvalues of $\boldsymbol{L}^{UI\Delta} = \boldsymbol{L}^{UI} (\Delta \oplus \Delta) \boldsymbol{L}^{IUd}$. Therefore, the stability of the equilibrium resting state is determined to a first order by the eigenvalues s_n^v of the corresponding sensitivity operator in the viscous case. Working in a similar way as in Appendix A, we use (B 6) and (B 9) to reduce the expression of the sensitivity operator to (6.1).

REFERENCES

Bamieh, B. & Dahleh, M. 2001 Energy amplification in channel flows with stochastic excitation. *Phys. Fluids* **13**, 3258–3269.

Berloff, P., Kamenkovich, I. & Pedlosky, J. 2009*a* A mechanism of formation of multiple zonal jets in the oceans. *J. Fluid Mech.* **628**, 395–425.

Berloff, P., Kamenkovich, I. & Pedlosky, J. 2009*b* A model of multiple zonal jets in the oceans: dynamical and kinematical analysis. *J. Phys. Oceanogr.* **39**, 2711–2734.

Bernstein, J. & Farrell, B. F. 2010 Low-frequency variability in a turbulent baroclinic jet: Eddy-mean flow interactions in a two-level model. *J. Atmos. Sci.* **67**, 452–467.

Bouchet, F. & Sommeria, J. 2002 Emergence of intense jets and Jupiter's Great Red Spot as maximum-entropy structures. *J. Fluid Mech.* **464**, 165–207.

Brewer, J. W. 1978 Kronecker products and matrix calculus in system theory. *IEEE Trans. Circuits Syst.* **9**, 772–781.

Charney, J. G. & DeVore, J. G. 1979 Multiple flow equilibria in the atmosphere and blocking. *J. Atmos. Sci.* **36**, 1205–1216.

Connaughton, C., Nadiga, B., Nazarenko, S. & Quinn, B. 2010 Modulational instability of Rossby and drift waves and generation of zonal jets. *J. Fluid Mech.* **654**, 207–231.

Davis, P. J. 1978 *Circulant Matrices*. Wiley-Interscience.

DelSole, T. 1996 Can quasigeostrophic turbulence be modeled stochastically? *J. Atmos. Sci.* **53**, 1617–1633.

DelSole, T. 1999 Stochastic models of shear-flow turbulence with enstrophy transfer to subgrid scales. *J. Atmos. Sci.* **56**, 3692–3703.

DelSole, T. 2001 A theory for the forcing and dissipation in stochastic turbulence models. *J. Atmos. Sci.* **58**, 3762–3775.

DelSole, T. 2004 Stochastic models of quasigeostrophic turbulence. *Surv. Geophys.* **25**, 107–194.

DelSole, T. & Farrell, B. F. 1995 A stochastically excited linear system as a model for quasigeostrophic turbulence: Analytic results for one- and two-layer fluids. *J. Atmos. Sci.* **52**, 2531–2547.

DelSole, T. & Farrell, B. F. 1996 The quasi-linear equilibration of a thermally maintained, stochastically excited jet in a quasigeostrophic model. *J. Atmos. Sci.* **53**, 1781–1797.

https://doi.org/10.1017/jfm.2011.228 Published online by Cambridge University Press

Diamond, P. H., Itoh, S. I., Itoh, K. & Hahm, T. S. 2005 Zonal flows in plasma – a review. *Plasma Phys. Control. Fusion* **47**, R35–R161.

Dijkstra, H. A. & Katsman, C. A. 1997 Temporal variability of the wind driven quasi-geostrophic double gyre ocean circulation: basic bifurcation diagrams. *Geophys. Astrophys. Fluid Dyn.* **53**, 195–232.

Duguet, Y., Schlatter, P. & Henningson, D. S. 2009 Localized edge states in plane Couette flow. *Phys. Fluids* **21**, 111701.

Faisst, H. & Eckhardt, B. 2003 Travelling waves in pipe flow. *Phys. Rev. Lett.* **91**, 224502.

Farrell, B. F. & Ioannou, P. J. 1993*a* Stochastic dynamics of baroclinic waves. *J. Atmos. Sci.* **50**, 4044–4057.

Farrell, B. F. & Ioannou, P. J. 1993*b* Stochastic forcing of perturbation variance in unbounded shear and deformation flows. *J. Atmos. Sci.* **50**, 200–211.

Farrell, B. F. & Ioannou, P. J. 1993*c* Stochastic forcing of the linearized Navier–Stokes equations. *Phys. Fluids* **5**, 2600–2609.

Farrell, B. F. & Ioannou, P. J. 1994 A theory for the statistical equilibrium energy spectrum and heat flux produced by transient baroclinic waves. *J. Atmos. Sci.* **51**, 2685–2698.

Farrell, B. F. & Ioannou, P. J. 1995 Stochastic dynamics of the midlatitude atmospheric jet. *J. Atmos. Sci.* **52**, 1642–1656.

Farrell, B. F. & Ioannou, P. J. 1996 Generalized stability theory. Part I: Autonomous operators. *J. Atmos. Sci.* **53**, 2025–2040.

Farrell, B. F. & Ioannou, P. J. 1998 Perturbation structure and spectra in turbulent channel flow. *Theor. Comput. Fluid Dyn.* **11**, 215–227.

Farrell, B. F. & Ioannou, P. J. 2003 Structural stability of turbulent jets. *J. Atmos. Sci.* **60**, 2101–2118.

Farrell, B. F. & Ioannou, P. J. 2007 Structure and spacing of jets in barotropic turbulence. *J. Atmos. Sci.* **64**, 3652–3655.

Farrell, B. F. & Ioannou, P. J. 2008 Formation of jets in baroclinic turbulence. *J. Atmos. Sci.* **65**, 3352–3355.

Farrell, B. F. & Ioannou, P. J. 2009*a* Emergence of jets from turbulence in the shallow-water equations on an equatorial beta-plane. *J. Atmos. Sci.* **66**, 3197–3207.

Farrell, B. F. & Ioannou, P. J. 2009*b* A stochastic structural stability theory model of the drift wave-zonal flow system. *Phys. Plasmas* **16**, 112903.

Farrell, B. F. & Ioannou, P. J. 2009*c* A theory of baroclinic turbulence. *J. Atmos. Sci.* **66**, 2444–2454.

Fujisawa, A., Itoh, K., Shimizu, A., Nakano, H., Ohshima, S., Iguchi, H., Matsuoka, K., Okamura, S., Minami, T., Yoshimura, Y., Nagaoka, K., Ida, K., Toi, K., Takahashi, C., Kojima, M., Nishimura, S., Isobe, M., Suzuki, C., Akiyama, T., Ido, T., Nagashima, Y., Itoh, S.-I. & Diamond, P. H. 2008 Experimental studies of zonal flow and field in compact helical system plasma. *Phys. Plasmas* **15**, 055906.

Gill, A. E. 1974 The stability of planetary waves on an infinite beta plane. *Geophys. Fluid Dyn.* **6**, 29–47.

Graham, A. 1981 *Kronecker Products and Matrix Calculus with Applications*. Ellis Horwood Ltd.

Huang, H. P., Galperin, B. H. & Sukoriansky, S. 2001 Anisotropic spectra in two-dimensional turbulence on the surface of a rotating sphere. *Phys. Fluids* **13**, 225–240.

Huang, H. P. & Robinson, W. A. 1998 Two-dimensional turbulence and persistent zonal jets in a global barotropic model. *J. Atmos. Sci.* **55**, 611–632.

Hunt, J. C. R. & Corruthers, D. J. 1990 Rapid distortion theory and the 'problems of turbulence. *J. Fluid Mech.* **212**, 497–532.

Hwang, Y. & Cossu, C. 2010 Amplification of coherent structures in the turbulent Couette flow: an input–output analysis at low Reynolds number. *J. Fluid Mech.* **643**, 333–348.

Ingersoll, A. P. 1990 Atmospheric dynamics of the outer planets. *Science* **248**, 308–315.

Ingersoll, A. P., Gierasch, P. J., Banfield, D. & Vasavada, A. R. 2000 Moist convection as an energy source for the large-scale motions in Jupiter's atmosphere. *Nature* **403**, 630–632.

Jeffreys, H. 1926 On the dynamics of geostrophic winds. *Q. J. R. Meteorol. Soc.* **52**, 85–104.

Jovanovic, M. & Bamieh, B. 2005 Componentwise energy amplification in channel flows. *J. Fluid Mech.* **534**, 145–183.

https://doi.org/10.1017/jfm.2011.228 Published online by Cambridge University Press

Kitamura, Y. & Ishioka, K. 2007 Equatorial jets in decaying shallow-water turbulence on a rotating sphere. *J. Atmos. Sci.* **64**, 3340–3353.

Krishnamurti, R. & Howard, L. N. 1981 Large-scale flow generation in turbulent convection. *Proc. Natl Acad. Sci.* **78**, 1981–1985.

Kuo, H.-L. 1951 Vorticity transfer as related to the development of the general circulation. *J. Meteorol.* **8**, 307–315.

Laval, J.-P., Dubrulle, B. & McWilliams, J. C. 2003 Langevin models of turbulence: Renormalization group, distant interaction algorithms or rapid distortion theory? *Phys. Fluids* **15**, 1327–1339.

Legras, B. & Ghil, M. 1985 Persistent anomalies, blocking and variations in atmospheric predictability. *J. Atmos. Sci.* **42**, 433–471.

Lorenz, E. N. 1974 Barotropic instability of Rossby wave motion. *J. Atmos. Sci.* **29**, 258–264.

Marshall, J. & Molteni, F. 1993 Toward a dynamical understanding of planetary-scale flow regimes. *J. Atmos. Sci.* **50**, 1792–1818.

Nazarenko, S. & Quinn, B. 2009 Triple cascade behavior in quasigeostrophic and drift turbulence and generation of zonal jets. *Phys. Rev. Lett.* **103**, 118501.

Newman, M., Sardeshmukh, P. D. & Penland, C. 1997 Stochastic forcing of the wintertime extratropical flow. *J. Atmos. Sci.* **54**, 435–455.

Nozawa, T. & Yoden, Y. 1997 Formation of zonal band structure in forced two-dimensional turbulence on a rotating sphere. *Phys. Fluids* **9**, 2081–2093.

Pierrehumbert, R. & Malguzzi, P. 1984 Forced coherent structures and local multiple equilibria in a barotropic atmosphere. *J. Atmos. Sci.* **41**, 246–257.

Rayleigh, Lord 1880 On the stability, or instability, of certain fluid motions. *Proc. Lond. Math. Soc.* **9**, 57.

Read, P. L., Yamazaki, Y. H., Lewis, S. R., Williams, P. D., Miki-Yamazaki, K., Sommeria, J., Didelle, H. & Fincham, A. 2004 Jupiter's and Saturn's convectively driven banded jets in the laboratory. *Geophys. Res. Lett.* **87**, 1961–1967.

Read, P. L., Yamazaki, Y. H., Lewis, S. R., Williams, P. D., Wordsworth, R. & Miki-Yamazaki, K. 2007 Dynamics of convectively driven banded jets in the laboratory. *J. Atmos. Sci.* **64**, 4031–4052.

Rhines, P. B. 1975 Waves and turbulence on a beta plane. *J. Fluid Mech.* **69**, 417–433.

Robert, R. & Sommeria, J. 1991 Statistical equilibrium states for two-dimensional flows. *J. Fluid Mech.* **229**, 291–310.

Salyk, C., Ingersoll, A. P., Lorre, J., Vasavada, A. & Del Genio, A. D. 2006 Interaction between eddies and mean flow in Jupiter's atmosphere: Analysis of Cassini imaging data. *Icarus* **185**, 430–442.

Shepherd, T. G. 1987 A spectral view of nonlinear fluxes and stationary–transient interaction in the atmosphere. *J. Atmos. Sci.* **44**, 1166–1178.

Simonnet, E., Ghil, M. & Dijkstra, H. A. 2005 Homoclinic bifurcations in the barotropic quasi-geostrophic double-gyre circulation. *J. Mar. Res.* **63**, 931–956.

Starr, V. 1968 *Physics of Negative Viscosity Phenomena.* McGraw Hill.

Vallis, G. K. & Maltrud, M. E. 1993 Generation of mean flows and jets on a beta plane and over topography. *J. Phys. Oceanogr.* **23**, 1346–1362.

Vasavada, A. R. & Showman, A. P. 2005 Jovian atmospheric dynamics. An update after Galileo and Cassini. *Rep. Prog. Phys.* **68**, 1935–1996.

Waleffe, F. 2003 Homotopy of exact coherent structures in plane shear flows. *Phys. Fluids* **15**, 1517–1534.

Wedin, H. & Kerswell, R. R. 2004 Exact coherent structures in pipe flow: travelling wave solutions. *J. Fluid Mech.* **508**, 333–371.

Whitaker, J. S. & Sardeshmukh, P. D. 1998 A linear theory of extratropical synoptic eddy statistics. *J. Atmos. Sci.* **55**, 237–258.

Zhang, Y. & Held, I. M. 1999 A linear stochastic model of a GCM's midlatitude storm tracks. *J. Meteorol. Soc. Japan* **56**, 3416–3435.

https://doi.org/10.1017/jfm.2011.228 Published online by Cambridge University Press